DESIGN, ANALYSIS AND TESTING OF CENTRIFUGAL SMALL CIRCULATOR PUMP CASING PRODUCED BY PLASTIC INJECTION METHOD

ABDULLAH KAYA

SEPTEMBER 2025

ÇANKAYA UNIVERSITY

GRADUATE SCHOOL

MECHANICAL ENGINEERING DEPARTMENT
MECHANICAL ENGINEERING MASTER'S THESIS

DESIGN, ANALYSIS AND TESTING OF CENTRIFUGAL CIRCULATION PUMP WITH CASING MANUFACTURED BY PLASTIC INJECTION TECHNIQUE

ABDULLAH KAYA

SEPTEMBER 2025

ABSTRACT

DESIGN, ANALYSIS AND TESTING OF CENTRIFUGAL CIRCULATION PUMP WITH CASING MANUFACTURED BY PLASTIC INJECTION TECHNIQUE

KAYA, ABDULLAH
MECHANICAL ENGINEERING MASTER'S THESIS

Supervisor: Assoc. Prof. Dr. HAŞMET TÜRKOĞLU
September 2025, 60 Pages

Since the current sand-casting technique is not suitable for the mass production of small-sized pumps, the composite-plastic pump casing designed for plastic injection molding constitutes an important part of this study. The designed pump casing has been optimized based on manufacturability, hydraulic efficiency, cost-effectiveness, weight, and suitability for mass production.

In this thesis study, a low-capacity circulation pump casing was designed, manufactured using a 3D printer, and tested. Various design criteria were defined and applied to different geometries to determine the most optimal and efficient design. Numerical analyses were performed using the ANSYS-CFX software (version 2021 R2) to optimize hydraulic efficiency and mechanical stress distribution. A test system was developed to validate the designs. All prototypes were tested step by step and compared with each other, and the most suitable design was determined in terms of efficiency and manufacturability.

Keywords: Circulator pump, hydraulic performance analysis, plastic pump casing

ÖZET

PLASTİK ENJEKSİYON TEKNİĞİYLE ÜRETİLEN GÖVDELİ SANTRİFÜJ SİRKÜLASYON POMPASININ TASARIMI, ANALİZİ VE TESTLERİ

KAYA, ABDUULAH
MAKİNE MÜHENDİSLİĞİ YÜKSEK LİSANS TEZİ

Danışman: Prof. Dr. Haşmet TÜRKOĞLU
Eylül 2025, 60 Sayfa

Mevcut kum döküm tekniği ile yüksek miktarlardaki küçük boyutlu pompaların üretimi elverişli olmadığından, plastik enjeksiyon yöntemine uygun olarak tasarlanan kompozit-plastik pompa gövdesi çalışmanın önemli bir parçasıdır. Tasarlanan pompa gövdesi, üretilebilirlik, hidrolik verimlilik, maliyet etkinliği, ağırlık ve seri üretime uygunluk temelinde optimize edilmiştir.

Tez çalışmasında, küçük kapasiteli bir sirkülasyon pompası gövdesi tasarlanmış, 3-boyutlu yazıcı kullanılarak üretilmiş ve test edilmiştir. Optimum ve en verimli tasarımı belirlemek için çeşitli tasarım kriterleri belirlenmiş ve farklı geometrilere uygulanmıştır. Hidrolik verimliliği ve mekanik gerilme dağılımını optimize etmek için ANSYS-CFX (2021 R2 versiyon) yazılım programı kullanılarak sayısal analiz yapılacaktır. Tasarımları doğrulamak için bir test sistemi geliştirilmiştir. Tüm prototipler adım adım test edilmiş ve birbirleriyle karşılaştırılarak, verim ve üretilebilirlik açılarından en uygun tasarım belirlenmiştir.

Anahtar Kelimeler: Sirkülasyon pompası, hidrolik performans analiz, plastik pompa gövdesi

ACKNOWLEDGEMENT

First, I am grateful to my family who have helped me this far, and to my dear teachers who contributed to my education. I would like to thank my wife and my dear daughter for their moral support. I would like to express my endless respects to our valuable teacher Prof. Dr. Haşmet TÜRKOĞLU who supported me in this thesis. I would also like to thank the KSB corporate family for their support.

TABLE OF CONTENTS

STATEMENT OF NONPLAGIARISM III
ABSTRACT IV
ÖZET V
ACKNOWLEDGEMENT VI
LIST OF TABLES IX
LIST OF FIGURES X
LIST OF SYMBOLS AND ABBREVIATIONS XII
CHAPTER I 1
INTRODUCTION 1
1.1 CENTRIFUGAL PUMP BASICS 2
1.2 CHARACTERISTIC PUMP PARAMETERS 3
1.2.1 Specific Work and Pump Head 3
1.2.2 Volume Flow Rate 5
1.2.3 Hydraulic Power 5
1.2.4 Shaft Power 5
1.2.5 Pump Efficiency Expressions 6
1.2.6 Leakage Efficiency 7
1.2.7 Hydraulic Efficiency 7
1.2.8 Mechanical Efficiency 8
1.3 IMPORTANCE OF SPIRAL CASING 8
1.3.1 Volute Tongue and Gap Ratio 10
1.4 LITERATURE SEARCH 11
CHAPTER II 13
PUMP HYDRAULIC DESIGN 13
2.1 CASING DESIGN 13
CHAPTER III 18
EXPERIMENTAL STUDY 18
3.1 EXPERIMENT TEST RIG 18
3.2 EXPERIMENTAL ERROR ANALYSIS 20
3.3 PERFORMING EXPERIMENTS AND DATA COLLECTION 22
3.4 ANALYSIS OF EXPERIMENTAL RESULTS 23
3.4.1 Effects of the Gap Distance (Δd) on Pump Performance 24

3.4.2 Effects of the Volute Outlet Size on Pump Performance ... 26
3.4.3 Effects of the Inclination Angle of Inlet Pipe on Pump Performance 28
3.4.4 Comparison of the optimized plastic casing with the casting casing . 30
CHAPTER IV ... 31
NUMERICAL STUDY ... 31
4.1 CREATING PUMP FLOW GEOMETRY ... 31
4.2 BASIC EQUATIONS ... 32
4.2.1 Reynolds Averaged Navier-Stokes (RANS) Equations ... 32
4.2.2 k-omega SST Turbulence Model ... 33
4.3 BOUNDARY CONDITIONS ... 34
4.4 NUMERICAL SOLUTION ... 34
4.4.1 Meshing and Preparing Model ... 35
4.5 NUMERICAL CALCULATION AND VALIDATION ... 37
4.5.1 Convergence, Iteration Independence and Mass Conservation Control ... 37
4.5.2 Independence of the Solution from the Number of Node ... 39
4.6 PERFORMANCE EVALUATION AND VALIDATION OF THE RESULTS ... 39
4.6.1 Torque and Shaft Power Calculation ... 40
4.6.2 Hydraulic Power Calculation ... 41
4.6.3 Pump Efficiency Calculation ... 41
4.7 MECHANICAL ANALYSIS ... 43
CHAPTER V ... 44
CONCLUSIONS ... 44
REFERENCES ... 45

LIST OF TABLES

Table 1: Pump design inputs 13
Table 2: Values of the characteristic parameters of the model casings 17
Table 3: Main elements and functions of the experimental setup. 19
Table 4: Experimental condition 20
Table 5: Allowed wave amplitude of the measured values....................................... 20
Table 6: The maximum resulting values of the total uncertainty of efficiency. 21
Table 7: The calculated errors 21
Table 8: Values of the parameters considered for experiments. 22
Table 9: The conservation of mass control values 38

LIST OF FIGURES

Figure 1: Centrifugal pump main parts 2
Figure 2: Circulation pump casting steel casing with inlet and outlet ports 3
Figure 3: Power terms on the pump 6
Figure 4: Volute casing 9
Figure 5: The spiral-volute flow geometry of cast iron casing 9
Figure 6: Casted pump casing and cross-section view with impeller 10
Figure 7: Flow volumes of the general view of the old and new design casings...... 14
Figure 8: View of the cross-sections of the new design casing with different inlet inclination angles, **a)** Model-1 with α_1=60° angle. **b)** Model-4 with α_2=76.5° angle.14
Figure 9: Casing cross-sections with different volute outlet size 16
Figure 10: 3-D printed casings, Model 1 to 5 from left to right 16
Figure 11: Tested pump with Model-4 17
Figure 12: Experiment test rig schematic 18
Figure 13: Photograph of the experimental test rig.. 19
Figure 14: Variation of pump power consumption with flow rate at different gap distances. (Inclination angle α_1=30°, Volute outlet size A_1=15.5 mm) 24
Figure 15: Variation of the pump head with flow rate at different gap distances..... 25
Figure 16: Variation of total pump efficiency with flow rate at different gap distances (Inclination angle 30°, Volute outlet size A_1= 15.5 mm).. 25
Figure 17: Variation of power consumption with flow rate at different volute outlet size. (Inclination angle α_1=30°, gap distance Δd=2.3 mm)....................................... 26
Figure 18: Variation of the pump head with flow rate at different volute outlet size. 27
Figure 19: Variation of total pump efficiency with flow rate at different volute outlet size. (Inclination angle α_1=30°, gap distance Δd=2.3 mm)....................................... 27
Figure 20: Variation of power consumption with flow rate at different inclination angles. (Volute outlet size A_1= 15.5 mm, gap distance Δd=2.3 mm)........................ 28

Figure 21: Variation of the pump head with flow rate at different inclination angle. 29
Figure 22: Variation of total pump efficiency with flow rate at different inclination angles........ 29
Figure 23: Efficiency results of the plastic pump casing and the casting pump casing 30
Figure 24: Flow volumes of the parts of the existing pump considered for the study. 32
Figure 25: Boundary conditions of injection molded pump casing pump model..... 34
Figure 26: Polyhedral mesh 36
Figure 27: Polyhedral mesh section view with the inflation layers 36
Figure 28: Orthogonal quality values and number of cells of polyhedral mesh 36
Figure 29: Hexagonal mesh 37
Figure 30: Head-pressure value and numbers of iteration graph 38
Figure 31: Residuals value and numbers of iteration graph 38
Figure 32: Independence of the solution from the number of node graph........ 39
Figure 33: Moment value and numbers of iteration graph 40
Figure 34: Pressure contours around the impeller for casting pump casing 42
Figure 35: Pressure contours around the pump for casting pump casing 42
Figure 36: The surfaces that applied pressure of 25 bar 43
Figure 37: Deformation and equivalent stress distribution on casing........ 43

LIST OF SYMBOLS AND ABBREVIATIONS

SYMBOLS

p	: Pressure [Pa]
Q	: Volume flow rate [m^3/h]
Q_l	: Leakage flow rate [m^3/h]
Q_i	: Flow rate leaves the impeller [m^3/h]
H	: Head [m]
V	: Velocity [m/s]
g	: Gravity [m/s^2]
ρ	: Density [kg/m^3]
N	: Rotational speed [rev/min]
P_m	: Shaft power [watt]
P_h	: Hydraulic power [watt]
$P_{L,hyd}$	: Hydraulic power loss [watt]
$P_{M,hyd}$	: Mechanic power loss [watt]
P_i	: Hydraulic power of the impeller (without losses) [watt]
P_d	: Hydraulic power at discharge [watt]
P_s	: Hydraulic power at suction [watt]
T_m	: Shaft torque [Nm]
d_2	: Impeller diameter [mm]
d_3	: Tongue diameter / Cutwater diameter [mm]
d_3^*	: Gap ratio
Y	: Specific work [J/kg]
h	: Enthalpy [J/kg]

Z	: Geodetic height [m]
η_p	: Pump efficiency (%)
η_l	: Leakage efficiency (volumetric efficiency) (%)
η_h	: Hydraulic efficiency (%)
η_m	: Mechanical efficiency (%)
η_T	: Total efficiency (%)
η_{em}	: Efficiency of the pump's electric motor (%)
η_{drv}	: Efficiency of the motor driver (%)
Δd	: The gap between tongue and impeller [mm]
μ	: Molecular(laminar) viscosity [Pa.s]
μ_t	: Turbulent viscosity [Pa.s]
k	: Turbulent kinetic energy [J/kg]
ε	: Turbulent kinetic energy dissipation rate
α	: Inclination angle at inlet
A	: Volute outlet size [mm]

ABBREVIATIONS

CFD	: Computational Fluid Dynamics
RANS	: Reynolds Average Navier-Stokes
SST	: Shear Stress Transport
SIMPLEC	: Semi-Implicit Method Pressure Linked Equations Consistent

CHAPTER I

INTRODUCTION

Centrifugal circulation pumps are used to circulate the existing fluid (water) in closed systems such as kombi boilers, boilers, heat sharing systems, and solar energy systems. These systems are widely used in domestic and in industrial heating applications. Due to their widespread and continuous use, the efficiency and cost of circulation pumps are crucial.

Generally, the casing of the circulation pumps is made by casting technique from metal materials and impellers are manufactured from plastic material by injection molding technique. Since manufacturing pump casing by casting technique from a metal (steel) material is expensive and has high negative environmental impact, it is desired to manufacture it by injection molding technique.

In this study, the casing of a single-stage existing circulator pump is redesigned so that geometrically it is suitable for plastic injection molding. As the manufacturability was a concern, hydraulic efficiency of the new pump was also an important concern in the design and analysis of the pump. To test the redesigned pump, an experimental setup is prepared. Five different casings were manufactured by the 3-D printing technique. Then, five different pumps with different casings but with the same impeller were tested experimentally to determine pump head, power consumption and efficiency.

Hydraulic analysis of the pumps with new design casings was also carried out numerically with the same impeller. For all new design pump casings, a three-dimensional solid model of the pump flow volume is created with the same impeller cavity. Using ANSYS-CFX software, the flow field and pump performance was numerically analyzed. To check the accuracy of the numerical results, experimental data obtained for the existing pump and the numerical results were compared.

Utilizing the results of the experimental and numerical analysis, the designed pump casing flow volume is optimized based on hydraulic efficiency, producibility, cost-effectiveness, weight and suitability for mass production by injection molding, and an optimum casing design is proposed

1.1 CENTRIFUGAL PUMP BASICS

A centrifugal pump is a rotating machine in which flow is generated, and pressure is increased by means of rotating blades. Generally, fluid enters axially into the pump, then it flows radially in the rotor and leaves the rotor through the diffuser. The pump in the recirculating systems creates enough pressure difference to overcome the self-resistance of the system at the desired flow rate.

In Fig. 1, a decomposed centrifugal circulation pump is shown. A centrifugal circulation pump consists of three main components: casing, impeller, and electric motor with housing that drives the shaft of the impeller. Casings are usually produced such that the inlet and outlet are in the same line for easy placement into the circulation line.

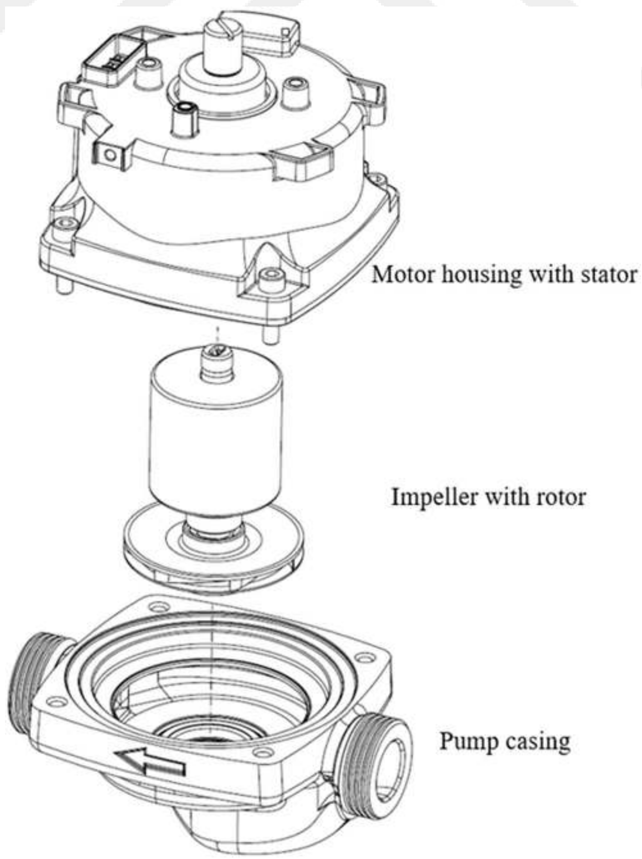

Figure 1: Centrifugal pump main parts (KSB Company 2025)

Impeller of the circulation pumps is generally manufactured by injection molding. However, the pump casing is generally manufactured by casting technique. A cast iron casing is shown on Fig. 2. Pump casings manufactured by casting technique increase the cost of the product. In order to reduce the cost, it is desired to manufacture the casing also by injection molding technique. To utilize the injection molding technique to manufacture the casing, it should be redesigned such that geometry becomes suitable for manufacturing by injection molding.

Figure 2: Circulation pump casting steel casing with inlet and outlet ports

For injection molding technique to be applied, sliding cores are moving tool parts which move through or between the main tools temporarily creating a volume for the plastic to flow around and then removed as the tools open. The sliding cores follow a straight path or a circular path to leave the tool cavity. The straight path is preferred for its simplicity and cost-effectiveness.

For the pump casing seen on Fig. 2, two sliding cores are needed to generate the inlet cavity and outlet cavity. To make a simpler mold, these sliding cores should move along a straight line. In this study, the plastic pump casing was designed such that sliding cores can move along a straight line.

1.2 CHARACTERISTIC PUMP PARAMETERS

1.2.1 Specific Work and Pump Head

The specific work Y (J/kg) is the total energy transmitted by the pump to the per unit mass of the fluid. Specific work Y is the difference between the energy of the fluid at the suction and the discharge nozzles for unit mass of the fluid. Specific work

Y is identical to the total isentropic enthalpy rise Δh_{tot} from the inlet to the outlet. In incompressible flows $Y = \Delta p_{tot}/\rho$.

Pump head, H (m), is practically used for the specific energy increase of the unit mass of the fluid from the inlet to the outlet. In practice, the head $H = Y/g$ is commonly used (also termed "total head"). It must be comprehended as specific *energy unit* (or specific work) (Gulich 2010:43).

$$Y = \Delta h_{tot} = gH \tag{1.1}$$

The pump head is a term that the hydraulic power or pump output power transmitted to the fluid. In other words, pump head is the maximum height that a pump can move the fluid. It can be explained by the Bernoulli equation in Eq. 1.2.

$$H = \frac{p_d - p_s}{\rho g} + \frac{V_d^2 - V_s^2}{2g} + Z_d - Z_s \tag{1.2}$$

In this equation, all energies are expressed as "energy heads" and subscripts *d* and *s* denote discharge and suction, respectively. The static pressure head p/(g ×ρ) is measurable at the suction and at the discharge nozzle. Z is the elevation head which is the measure of the potential energy of the fluid at pump inlet and outlet. $V^2/(2g)$ is called velocity head. Head and specific work don't vary with density or type of medium. Thus, theoretically, a pump delivers the same head in pumping water, mercury or air. But doesn't develop the same pressure rise Δp=ρ×g×H as would be measured by a differential manometer. All pressure differences, powers, forces and stresses are proportional to the density (Gulich 2010:45).

For the specific condition of a pump that has same inlet and outlet diameter and same geodetic height, the head can be expressed as in Eq. 1.3.

$$H = \frac{p_d - p_s}{\rho g} \tag{1.3}$$

In the above equations, the symbols represent:

ρ Density of the fluid (kg/m³)

g Gravitational acceleration (m/s²)

H Pump head (m)

p_d Pump discharge pressure (Pa)

p_s Pump suction pressure (Pa)

Y Specific work (J/kg)

Z_d Geodetic height at discharge (m)

Z_s Geodetic height at suction (m)

V Flow velocity (m/s)

To deliver the specified volumetric flow rate through a given plant pump, the pump must supply a specific head known as the plant required head H. It is calculated from the extended Bernoulli's equation considering all the system head losses (other than pump losses).

1.2.2 Volume Flow Rate

The volumetric flow rate Q (m3 /s) is generally described as the effective volume flow through the discharge nozzle.

1.2.3 Hydraulic Power

Hydraulic power P_h (W) is the power transferred to the fluid by the pump impeller, and this power creates a pressure increase (head) in the fluid. P_h can be calculated from Eq. 1.4 using the values of volume flow rate Q (m^3/s), head H (m), gravitational acceleration g, and the density of the fluid ρ.

$$P_h = \rho\, g\, H\, Q \tag{1.4}$$

1.2.4 Shaft Power

The shaft power of the pump, P_m (W), is given in Eq. 1.5 in terms of the torque applied to the shaft, T_m (Nm), and the rotation speed, N (rpm).

$$P_m = T_m\, N\ 2\pi/60 \tag{1.5}$$

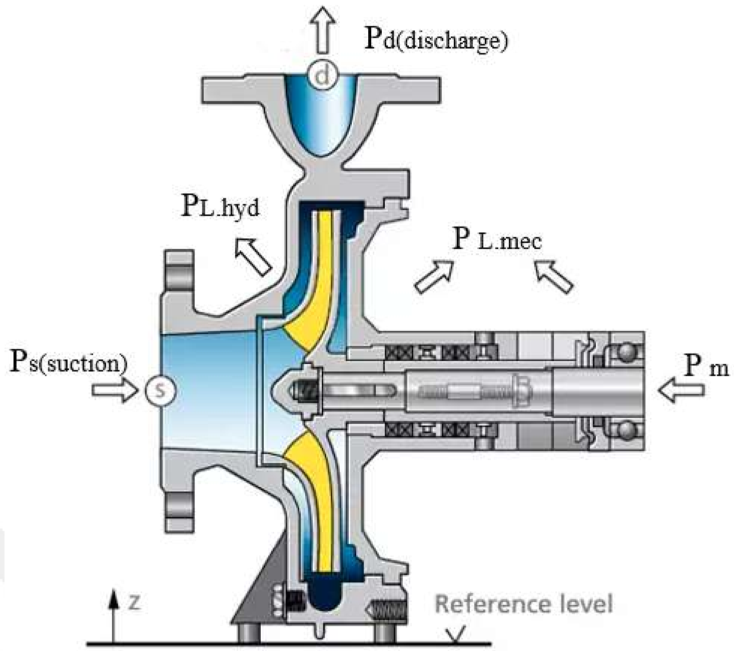

Figure 3: Power terms on the pump (KSB Company 2025)

The power output of the pump and power losses can be explained with Eq. 1.6, which is illustrated in Fig. 3.

$$P_h = P_d - P_s = P_m - P_{L.mec} - P_{L.hyd} \qquad (1.6)$$

P_h : Hydraulic power transferred to the fluid (W)

P_d : Hydraulic power at discharge (W)

P_s : Hydraulic power at suction (W)

P_m : Power transmitted to the shaft of the pump (W)

$P_{L.mec}$: Power losses in the pump bearings and shaft seal (W)

$P_{L.hyd}$: Hydraulic power loss (W)

1.2.5 Pump Efficiency Expressions

Based on the fact that the pump is a hydraulic machine that converts shaft power P_m into hydraulic power P_h, the pump efficiency η_p(%) in its most general form is written in Eq.1.7.

$$\eta_p = 100 \times \frac{P_h}{P_m} \qquad (1.7)$$

Here;

η_p : Pump efficiency (%)

P_h : Hydraulic power transferred to the fluid (W)

P_m : Power transmitted to the shaft of the pump (W)

In addition, in order to present and calculate the pump efficiency expressions in more detail, the pump efficiency is divided into leakage efficiency, hydraulic efficiency and mechanical efficiency components, and each component is examined separately. Pump efficiency components are expressed in Eq. 1.8.

$$\eta_p = \eta_l \eta_h \eta_m \tag{1.8}$$

η_l : Leakage efficiency (volumetric efficiency)

η_h : Hydraulic efficiency

η_m : Mechanical efficiency

1.2.6 Leakage Efficiency

The leakage efficiency η_l represents the loss due to the leakage flow rate returned to the impeller suction port after the fluid leaves the impeller. The leakage efficiency is expressed in Eq. 1.9.

$$\eta_l = \frac{Q}{Q_i} = \frac{Q}{Q + Q_l} \tag{1.9}$$

Q : Net volume flow rate (m^3/h)

Q_i : Volume flow rate leaves the impeller (m^3/h)

Q_l : Leakage volume flow rate (m^3/h)

1.2.7 Hydraulic Efficiency

Hydraulic efficiency η_h represents the head losses due to friction and local losses caused by fluid occurring in the impeller and the casing. The energy converted to heat does not lead to any increase in the pump power output. Hydraulic efficiency is expressed in Eq. 1.10.

$$\eta_h = \frac{P_i - P_{L.hyd}}{P_i} = 1 - \frac{P_{L.hyd}}{P_i} \qquad (1.10)$$

P_i : Power transmitted to the impeller (without losses) (W)

$P_{L.hyd}$: Hydraulic power loss (W)

1.2.8 Mechanical Efficiency

Mechanical efficiency represents the power losses caused by friction in the pump bearings and shaft seal. Mechanical efficiency is expressed in Eq. 1.11.

$$\eta_m = \frac{P_m - P_{L,mec}}{P_m} \qquad (1.11)$$

P_m : Power transmitted to the shaft of the pump (W)

$P_{L.mec}$: Power losses in the pump bearings and shaft seal (W)

1.3 IMPORTANCE OF SPIRAL CASING

Figure 1.4 illustrates volute casing adopted in pumps. Spiral or volute casing is a suction passage located in front of the impeller inlet and a delivery passage located behind the impeller outlet. In the volute casing, useful static pressure is created from the kinetic energy at the impeller outlet with minimal losses. Then, the volute casing supplies the fluid to the discharge section.

Under the optimum conditions, the flow in the pump impeller is axisymmetric. Hence, an axisymmetric and equal velocity distribution of flow around the volute should be ensured. Considerable radial forces may develop during operation at off-design conditions through disturbances of the circumferential symmetry of the flow in the casing. The radial forces create extra bearing loads, shaft bending stresses, and shaft deflection, which can affect the reliability of the pump.

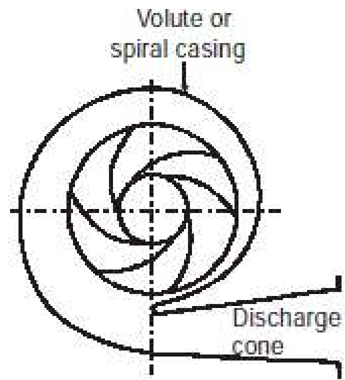

Figure 4: Volute casing (Srinivasan 2008:130)

The spiral helical flow geometry has a structure where the cross-sectional area perpendicular to the flow from the helical tongue to the helical exit expands linearly. Spiral casing at outlet comprises spiral shaped channel 0, 90°, 180°, 270°, 360° followed by a discharge cone 360°– 45°′ (Figure 5). The spiral section connects the impeller outlet to the discharge section 360°– 45°′ under axisymmetric flow.

Spiral casing not only accumulates the fluid leaving around the circumference of the impeller but also converts about 75% kinetic energy into pressure energy. The other 25% kinetic energy is converted on discharge suction. Volute casing plays an important role in hydraulic and total efficiency. (Srinivasan 2008:131)

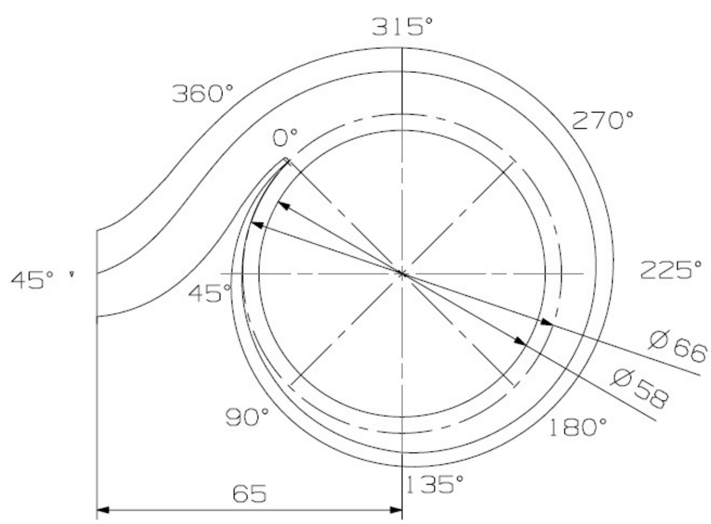

Figure 5: The spiral-volute flow geometry of cast iron casing

1.3.1 Volute Tongue and Gap Ratio

In Fig. 6, the casing tongue diameter, d_3, and the impeller diameter, d_2, are shown. The d_3 is also called volute cutwater diameter. The gap (Δd) between tongue and impeller diameters is equal to half of the difference between tongue diameter and impeller diameter ($\Delta d = (d_3 - d_2)/2$). The ratio of the tongue to the impeller diameter is called gap ratio ($d_3^* = d_3/d_2$). The tongue and the gap (Δd) are shown on the pump casing and impeller in Figure 6.

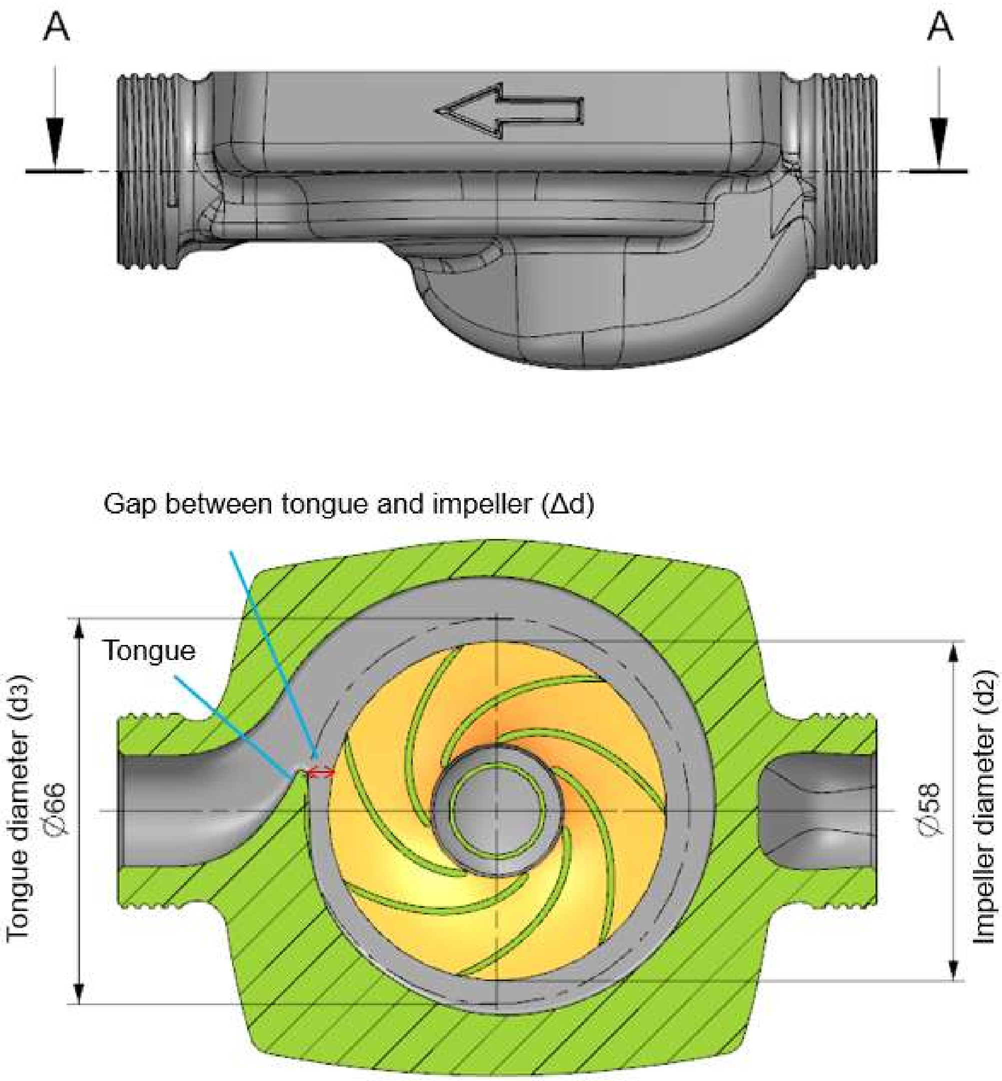

Figure 6: Casted pump casing and cross-section view with impeller

1.4 LITERATURE SEARCH

In this chapter, studies found in the literature about the pump casing design and analysis are summarized. Ozturk (2008) investigated the effect of the radial gap ratio (d_3^*) between the impeller and diffuser in a centrifugal pump. In this study, analyses were performed with three different radial gap ratios for 15 flow rates. It was observed that pressure fluctuations increase proportionally between the tongue and the diffuser when the gap decreases.

The effect of space between the impeller exit diameter and volute tongue is analyzed by Fernandez *et al.* (2023). How the radial gap size (Δd) effects the unsteady fluctuations of the velocity field in the pump is investigated. The four different radial gaps considered and analysis were performed at five flow rates. These radial gaps are achieved by using different impeller outer diameters. The pump volute casing was the same for all cases. Three different locations of tongue geometry are analyzed by Mahdi *et al.* (2022). The angle of the tongue is changed according to volute exit. The size of pressure fluctuations compared for each different tongue location.

Karakaya (2022) analyzed the effect of cutwater diameter on pump performance for four different cutwater diameters. The pressure distributions are obtained by numerical analysis. The efficiency of the pump is determined for every case with the same flow rate. The impeller diameter-volute cutwater gap (Δd) is one of the most important design variables to limit the pressure pulsations generated under high circumferential velocity to a tolerable value and avoiding fatigue cracks of impeller, or other components. Pressure pulsations and unsteady stresses are proportional to $(d3/d2\text{-}1)^{-0.77}$ according to Gülich's (2010:561) research. Doubling the gap thus reduces excitation forces by about 40%. But this is true only if a specific impeller is coupled with different diffusers of different inlet diameters. Trimming the impeller for increasing the gap, increases the blade loading to the effect that the benefits of an enlarged the gap can be less than stipulated above. As a rule, however, it can be justly assumed that impeller trimming will reduce pressure pulsations, especially in diffuser pumps. In sporadic cases, a gap widening can also lead to more pulsations, as demonstrated from tests on a volute pump. This effect is caused by a more uneven impeller outlet flow distribution because of higher vane loading and maybe thicker trailing edge blades. Volute pumps are more prone to such deviant conduct than diffuser pumps (since the gap is large, the relative gain due to trimming in the form of $(d3/d2\text{-}1)^{-0.77}$ is small and the influence of increased blade loading might prevail). According to Gülich (2010:424), the gab (Δd) is to be continued between impeller and volute tongue in order to limit pressure pulsations and hydraulic excitation forces to an acceptable level. The gab ratio (d3*) may be calculated from the formula given in Eqn. 2.1. A minimum diametrical clearance of 2 mm can be applied for small impellers with d3 = d2+2 mm, but only if this does not conflict with the requirements given in Eqn.2.1.

The impeller- volute interface in a centrifugal pump analyzed by Mentzos *et al.* (2004). The standard k-ϵ turbulence model is used to simulate turbulence. The analysis is explained detailly for a good foundation for the future work. The study is useful for basically understanding the flow contour in various design points. The CFD results compared with experimental results for three different side clearance widths between semi-open impeller hub and volute casing by Ayad *et al.* (2015). The impeller side clearance has a big effect on the centrifugal pump performance. When the flow mixed with the core flow, the pressure rise decreased because of flow blocking.

Özbilgin (2017) investigated the effect of the pump casing cross-sectional size on the centrifugal pump performance. In the study, the five different speeds of the impeller and three different volte areas are numerically analyzed. The numerical simulation is validated by using the existing pump experiment result. The centrifugal pump was designed according to desired working point with maximum efficiency by Nandan *et al*. (2023). In this study, all the numerical analysis steps in Ansys CFX are introduced clearly. The impeller and volute casing designed. The effect of the blade angle on the pump efficiency was analyzed numerically.

CHAPTER II
PUMP HYDRAULIC DESIGN

In pump design, the values of the pump characteristic parameters are determined based on the expected usage needs of the pump. These values are flow rate Q, discharge head H and impeller rotational speed N values. In determining these values, the values that will work for the longest time in the pump's life or the values that will most suit more than one value at which will work for the longest time are taken as the most efficient operating point of the pump. This point is the design point. The pump is designed to provide the highest efficiency at this point.

In the design made within the scope of this thesis, the values given in Table 1 were taken as design inputs.

Table 1: Pump design inputs

Parameter	**Value**
Flow rate	2.4 m^3/h
Head	7 m
Speed	3750 rpm
Fluid (Temperature)	Water (20°C)
Pump inlet-outlet pipe nominal diameter	DN20 – 3/4″
Pump material	Plastic
Distance between inlet and outlet	130 mm

In this study, an existing impeller is considered, and volute (spiral) is redesigned so that it can be manufactured by injection molding technique. Hence, in this chapter, the design of the volute is explained only. Different volute geometries are formed.

2.1 CASING DESIGN

In this study, the new design casings are obtained by modifying the casing of an existing pump already being manufactured by KSB company. A flow volume model of the volute of the existing pump considered for this study is shown in Fig. 7-a. To obtain a casing which can be manufactured by injection molding technique, the existing casing was modified. For this purpose, the curved sections like intake and diffuser sections (shown in Fig. 7-a), which cause problems in injection molding manufacturing technique, are redesigned to eliminate the curved surfaces (shown in Fig. 7-b).

In new models, inlet and diffuser sections are designed straight and inlet pipe is connected to axially at the impeller eye with an angle as shown in Fig. 7-b. As shown in the technical drawing of the casing given on Fig. 8, two different inclination angles between the axis of the pump and inlet pipe were considered. Two different angles were considered as 60° and 76.5° degrees.

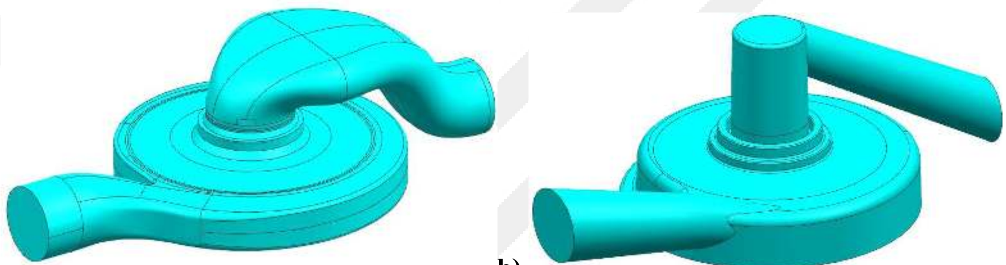

a) **b)**

Figure 7: Flow volumes of the general view of the old and new design casings. **a)** Old casing, **b)** New casing

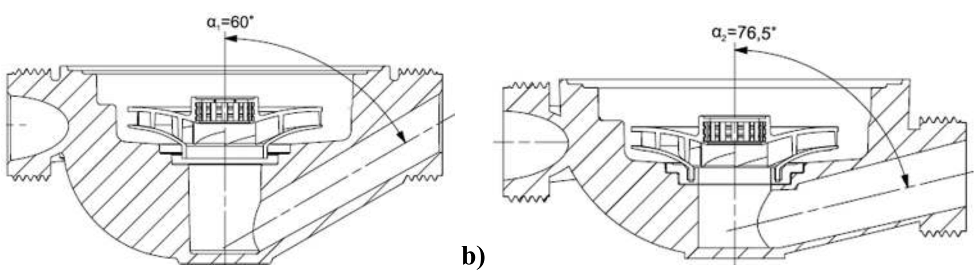

a) **b)**

Figure 8: View of the cross-sections of the new design casing with different inlet inclination angles, **a)** Model-1 with α_1=60° angle. **b)** Model-4 with α_2=76.5° angle.

In addition, in the new design, two different design modifications were also considered. These are the different gap distance (Δd) and the volute outlet size (A). The first modification on the casing was the gap distance (Δd) between the impeller and tongue. The casing was designed such that, casing with gaps Δd=0.9, 2.3 and 3.7 were obtained.

The volute cutwater diameter, d_3 (tongue diameter), can be found using Eq. 2.1 according to Gulich (2010:567).

$$\frac{d_3}{d_2} \geq 1.03 + 0.1\frac{n_q}{n_{q,ref}} + 0.07\frac{\rho\, H_{st}}{\rho_{ref}\, H_{ref}} \tag{2.1}$$

$n_{q\ ref}$: 40

H_{ref} : 1000 m

ρ_{ref} : 1000 kg/m^3

The specific speed n_q can be found using the Eq. 2.2.

$$\mathrm{nq} = \frac{N\sqrt{\mathrm{Q}}}{\mathrm{H}^{0,75}} \tag{2.2}$$

$$\mathrm{nq} = \frac{3750\sqrt{2.4/3600}}{7.8^{0,75}}$$

$$\mathrm{nq} = 20.7$$

The minimum required d_3 can be calculated from the equation 2.1.

$$\frac{d_3}{58} \geq 1.03 + 0.1\frac{20.7}{40} + 0.07\frac{1000\ x\ 7}{1000\ x\ 1000}$$

$$d_3\ = 62.77\ \mathrm{mm}$$

The tongue diameter d_3 were obtained as 59.8, 62.6 and 65.4 for the gaps 0.9, 2.3 and 3.7 mm. As understood, 62.6 mm is very close to 62.77 mm that is calculated from the equation 2.1. The Δd=2.3 mm is the optimum value according to the Eq. 2.1. In this study, this theoretical optimum value will be validated by an experimental method.

The second modification on the casing is the volute outlet size (A). Two volute outlet sections of different sizes were designed as shown in Fig. 9.

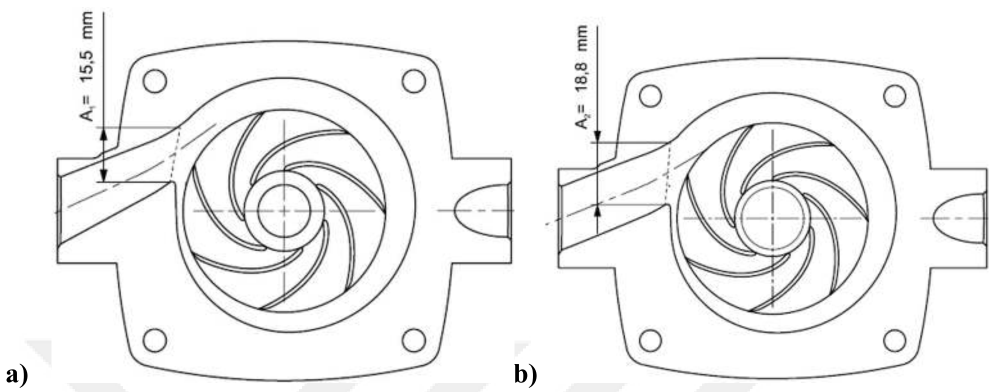

Figure 9: Casing cross-sections with different volute outlet size
a) Volute outlet size A_1 is 15.5 mm **b)** Volute outlet size A_2 is 18.8 mm.

With different values of inclination angle, impeller-tongue gap and volute outlet size, in total 5 different casing models were designed and manufactured by 3-dimensional printing technique. Casing models manufactured by 3-D printing technique are given in Fig. 10 and characteristics parameters of these models are given in Table 2.

Figure 10: 3-D printed casings, Model 1 to 5 from left to right

Table 2: Values of the characteristic parameters of the model casings

Model Number	Inclination angle of inlet pipe 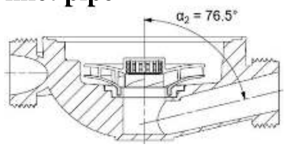	Tongue gap (mm) 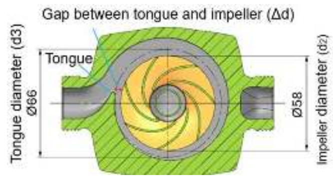	Volute outlet size (mm) 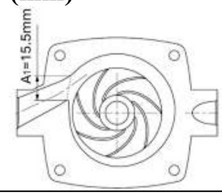
Model-1	$\alpha_1 = 60°$	$\Delta d = 3.7$	$A_1 = 15.5$
Model-2	$\alpha_1 = 60°$	$\Delta d = 2.3$	$A_1 = 15.5$
Model-3	$\alpha_1 = 60°$	$\Delta d = 0.9$	$A_1 = 15.5$
Model-4	$\alpha_2 = 76.5°$	$\Delta d = 2.3$	$A_1 = 15.5$
Model-5	$\alpha_1 = 60°$	$\Delta d = 2.3$	$A_2 = 18.8$

Figure 11: Tested pump with Model-4

CHAPTER III
EXPERIMENTAL STUDY

An experimental test setup is used to test the hydraulic performance of the pump casings, which are designed and manufactured using 3-D printing technique. The experiments are carried out with five different casing models given in Table 1. In this chapter, experimental setup, tests, data analysis, and experimental results are given.

3.1 EXPERIMENT TEST RIG

With the support of KSB Pump Company, a test system was established to obtain the experimental data of the pump. The schematic representation of the test system is given in Figure 12. The components of the system and their functions are explained in Table 3. In addition, a photograph of the physical state of the experimental setup is given in Figure 13.

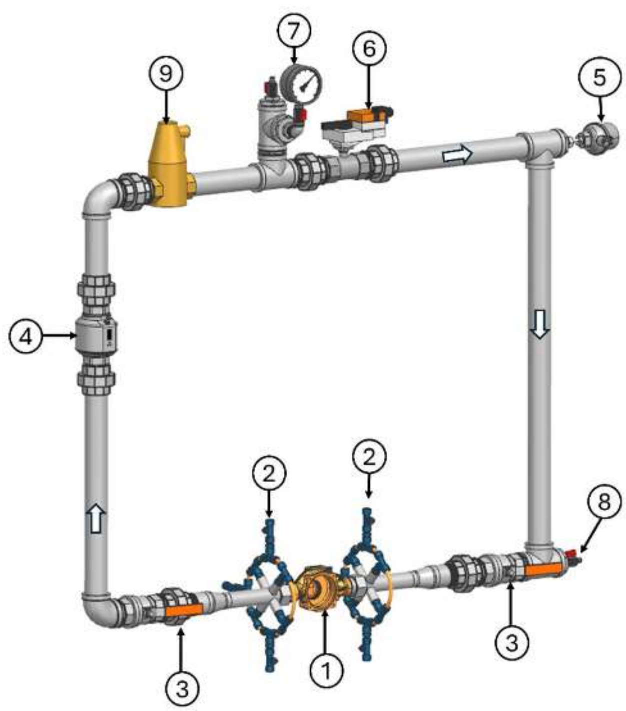

Figure 12: Experiment test rig schematic

Table 3: Main elements and functions of the experimental setup.

No	System component	Intended use
1	Pump (3750 rpm fixed speed setting)	Product to be experimentally examined
2	Pressure measuring transmitter (Product code: MBS 1700, measuring range: 0-25 bar, accuracy: ± % 0.5)	Measures the pressure at the inlet and outlet; the values are used to calculate the head difference
3	Ball valve	Insulation for pump removal and installation
4	Digital magnetic flowmeter (Product code: SM2130, measuring range: 0.05-54 m^3/h, accuracy: ± % 0.8)	Flow rate measurement
5	Resistance thermometer (Product code: OR01-PT100)	Water temperature measurement
6	Actuator valve (Product code: NR24A-SR, accuracy: ± % 5)	Adjusting the desired flow rate by controlling the valve
7	Manometer (Product code: MG040, measuring range: 0-40 bar, accuracy: ± % 2.5)	System pre-pressure (static) measurement
8	Mini ball valve	Loading fluid into the system
9	Air separator (Product code: 30016)	Venting air in the test rig while the pump is running for a good pressure measurement accuracy
Other	PVC or Brass material pipes, fittings, reducers, elbows etc. various connecting elements	Connecting system components together

Figure 13: Photograph of the experimental test rig.

Table 4: Experimental condition

Pump speed	3750 rev/min
Power supply	65 W
Flow rate	0 to 2.4 m^3/h in 0.2 intervals
Water temperature	20 °C
Ambient temperature	25 °C

The test setup shown in Fig. 13 was made ready for use by connecting the circulation pump (1). The system consists of a digital flow meter (4), pressure transmitters at the inlet and outlet (2), valves before and after the pump (3), an actuator-controlled valve (6), and other auxiliary components. In addition, the power drawn by the pump from the network ($P_{network}$) was read from the PLC screen. The pressure at the inlet and outlet of the pump was measured by transmitters. Then the software program is calculating head H, which can be seen on the PLC screen.

3.2 EXPERIMENTAL ERROR ANALYSIS

Even when measurement processes and equipment used, and analysis methods, are fully consistent with best practice and the requirements of this standard, there is always some uncertainty in any measurement. This uncertainty must be estimated with reasonable reliability. The criteria about the range of uncertainty are given in Tab. 5. according to Turkish Standard Institute (TSE) standards. (TS EN ISO 9906 2012: 11)

Table 5: Allowed wave amplitude of the measured values

Measured Value	**Allowed Wave Amplitude**		
	Class 1 (%)	**Class 2 (%)**	**Class 3 (%)**
Volume flow rate	±2	±3	±6
Pressure difference	±3	±4	±10
Exit pressure	±2	±3	±6
Inlet pressure	±2	±3	±6
Inlet power	±2	±3	±6
Revolution speed	±0.5	±1	±2
Torque	±2	±3	±6
Temperature	±0.3°C	±0.3°C	±0.3°C

A minimum of three (3) values should be taken at each test point. The random term e_R is to be calculated as per the following.

There are n number of readings, the arithmetic mean of the replicated sets of observations x_i (i=1…n), $\bar{x}$;

$$\bar{x} = \frac{1}{n} \Sigma x_{\hat{\imath}} \tag{3.1}$$

The standard deviation, s, of these observations is obtained by the following relation:

$$s = \sqrt{\frac{\perp}{n-1} \Sigma (x_i - \bar{x})^2} \tag{3.2}$$

The relative importance of the uncertainty in the mean due to random effects, e_R, is obtained by the following relation:

$$e_R = \frac{100\, t_s}{\bar{x}\sqrt{n}} \% \tag{3.3}$$

The total uncertainty value, *e*, is obtained by the following relation:

$$e = \sqrt{e_R^2 + e_S^2} \tag{3.4}$$

The total uncertainty of the overall efficiency and the pump efficiency is given by Equation 3.5.

$$e_n = \sqrt{e_Q^2 + e_H^2 + e_{Pnetwork}^2} \tag{3.5}$$

Table 6: The maximum resulting values of the total uncertainty of efficiency.

Value	**Symbol**	**Class 1 (%)**	**Class 2 (%)**
Total Efficiency (Calculating from Q, H, $P_{network}$)	e_n	±2.9	±6.1

The calculation of the errors for each measured value for volume flow rate Q, head H, power $P_{network}$, and total efficiency is given in Tab. 7. It is seen that our test ring complies with the standard that gives maximum values in Tab. 6.

Table 7: The calculated errors

Symbol	Calculated Values (%)
e_Q	3.36
e_H	1.43
$e_{Pnetwork}$	1.39
e_n	3.9

3.3 PERFORMING EXPERIMENTS AND DATA COLLECTION

Using the test set up given above, circulation pumps with different casings were tested to investigate the effects of the tongue ratio, inlet pipe inclination angle and volute outlet size on the performance of the pump. To perform this experimental analysis, pumps with 5 different casing models given above were mounted to the test system and measurements were made under different flow rates. The tests were carried out for the values of the parameters given in Table 8.

Table 8: Values of the parameters considered for experiments.

Parameter	**Value**	**Explanation**
Impeller speed (rpm)	3750	For all the tests kept constant
Water Temperature (°C)	20	For all the tests kept constant
Ambient temperature (°C)	25	For all the tests kept constant
Flow rate (m^3/h)	0.2, 0.4, 0.6, 0.8, 1, 1.2, 1.4, 1.6, 1.8, 2, 2.2 and 2.4	For all the cases, tests are performed with these flow rates.
Tongue ratio, Δd (mm)	0.9, 2.3 and 3.7	Impeller is the same, casing changed.
Volute outlet size, A (mm)	15.5 and 18.8	Impeller is the same, casing changed.
Inclination angle of the inlet pipe, α	60° and 76.5°	Impeller is the same, casing changed.

For each test, first, the pump to be tested is connected to the system, valves (3) are opened. Water with a pressure of a minimum of 2 bars and a maximum of 4 bars is filled into the system from valve 8. When the water starts to flow continuously, air bubbles in the water are released from the air separator (9). After air release is completed, valve 8 is closed and it is waited until the static pressure increase of the system stops in the manometer (7). The test system is ready for use when 2 bar static pressure is provided in the manometer (7). When the pump to be tested is to be changed, the change is made by closing the valves (3), and after the change, the ball valves (3) are opened and all the operations to make it ready for use are repeated.

The test setup in Figure 12 was made ready for use by connecting the circulation pump. First, the pump was operated at a fixed 3750 rpm while the actuator valve (6) was fully closed. In this case, the value of 0 m^3/h was read in the flowmeter (4). In addition, the power drawn by the pump from the network ($P_{network}$) and the total pressure difference (head H) at the inlet and outlet of the pump were read on the PLC screen. Then, the actuator valve (6) was brought to the half-closed positions so that the flow values of 0.2, 0.4, 0.6, 0.8, 1, 1.2, 1.4, 1.6, 1.8, 2, and 2.2 m^3/h were read on the flow meter (4), respectively.

When the test is started and the desired flow rate is seen on the flow meter, then the $P_{network}$ and the head (H) values are recorded that are seen on the PLC screen. All the pump casing models are tested by following this procedure step by step.

First, model-1, model-2 and model-3 are connected to the test rig step by step, and performance results are recorded to determine the influence of the impeller-volute tongue interface gap (Δd) differences. After this step, the optimum gap (Δd) can be determined.

In the second step, model-4 is connected to the test rig, and its results are compared with model-2. These two models have the same impeller-volute tongue gap (Δd) and same volute outlet size (A) but different inclination angle (α). The influence of the inlet inclination angle is analyzed with this step.

In the third step, model-5 is connected to the test rig, and its results are compared with model-2. These two models have the same impeller-volute tongue gap (Δd) and same inlet inclination angle (α) but different volute outlet size (A). This comparison gives us the influence of the cross-sectional area value on the performance.

In the experiments, the pump is run at 3750 rev/min speed. The electronic driver limits the power supply to 65 W. The volumetric flow rate is changed from 0 to 2,4 m^3/h. During the experiments, the same speed and flow rate values are used to compare the head (m) values of the different models.

3.4 ANALYSIS OF EXPERIMENTAL RESULTS

For the determined 13 different flow rates, the power drawn $P_{network}$ from the network by the pump and the pump's discharge head H values were measured. Experiments were repeated with all flow rates for 5 different casings. Using the measured power consumption and pressure increase in the pump, pump efficiencies are calculated as follows:

The hydraulic power of the pump (P_h) is calculated from Eq. 1.4. The total efficiency of the pump η_T is calculated as taking the ratio of the hydraulic power P_h to the power $P_{network}$ drawn from the network as given in Eq. 3.6. In addition, the total efficiency η_T can also be expressed in terms of the efficiency of the electric motor

η_{em}, the efficiency of the motor driver η_{drv} and the efficiency of the pump η_p as in Eq.3.7. Then, combining Eq. 3.6 and 3.7, the pump efficiency can be expressed as in Eq. 3.8.

$$\eta_T = 100 \times \frac{P_h}{P_{network}} \tag{3.6}$$

$$\eta_T = \eta_{em}\, \eta_{drv}\, \eta_p \tag{3.7}$$

$$\eta_P = 100 \times \frac{\rho\, g\, H\, Q}{P_{network}\, \eta_{em}\, \eta_{drv}} \tag{3.8}$$

3.4.1 Effects of the Gap Distance (Δd) on Pump Performance

Variations of power consumption, pump head and total pump efficiency with flow rate at different gap distances are plotted in Figs. 14, 15, and 16, respectively. As seen in these graphs, the Δd (2.3 mm) has higher head values and lower consumed power. As a result, efficiency is 2-3 percent better than the model has Δd (3.7 mm) as shown in Figure 16. On the other hand, the model has a gap Δd (0.9 mm), has a lower efficiency when compared to the other two models.

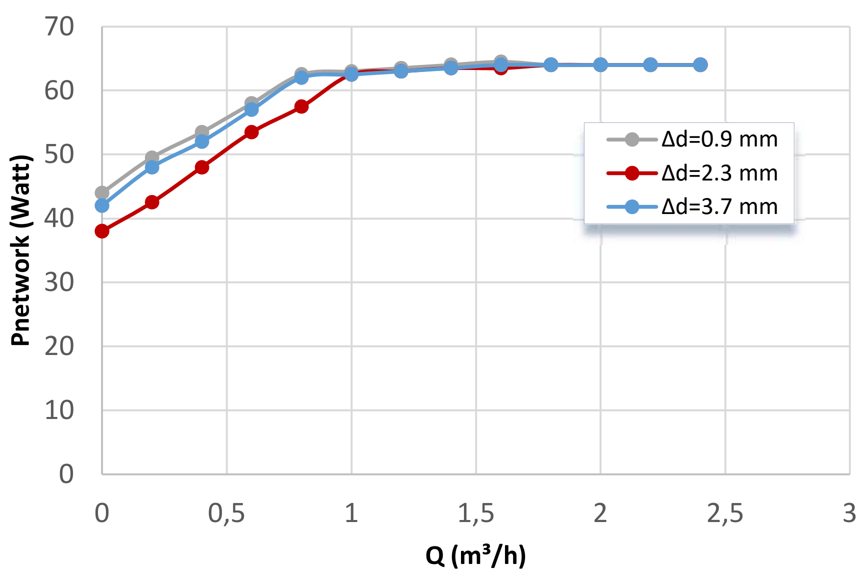

Figure 14: Variation of pump power consumption with flow rate at different gap distances. (Inclination angle α_1=30°, Volute outlet size A_1=15.5 mm)

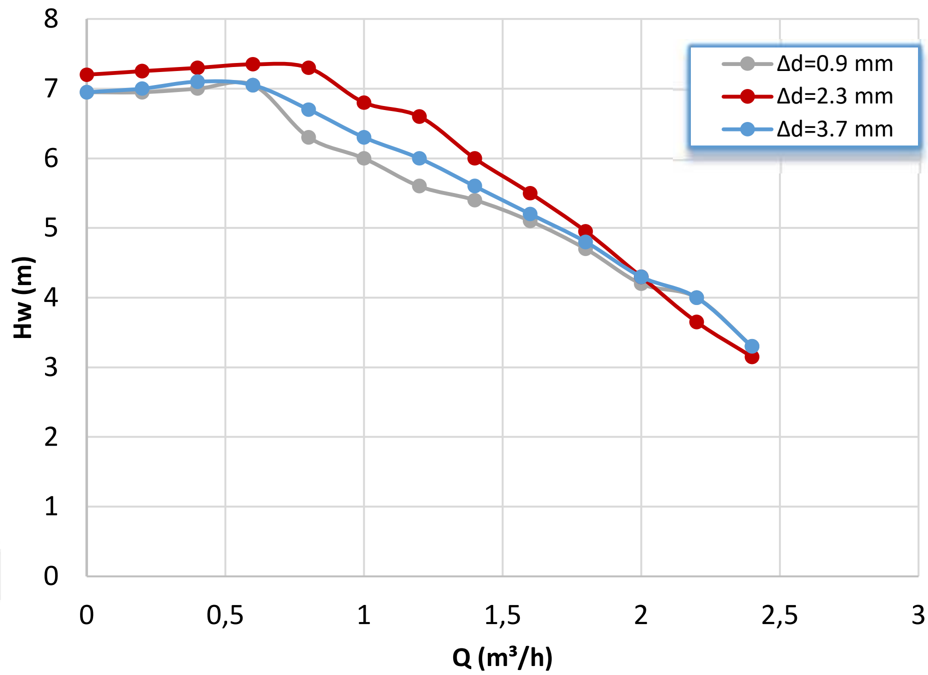

Figure 15: Variation of the pump head with flow rate at different gap distances. (Inclination angle α_1=30°, Volute outlet size A_1=15.5 mm)

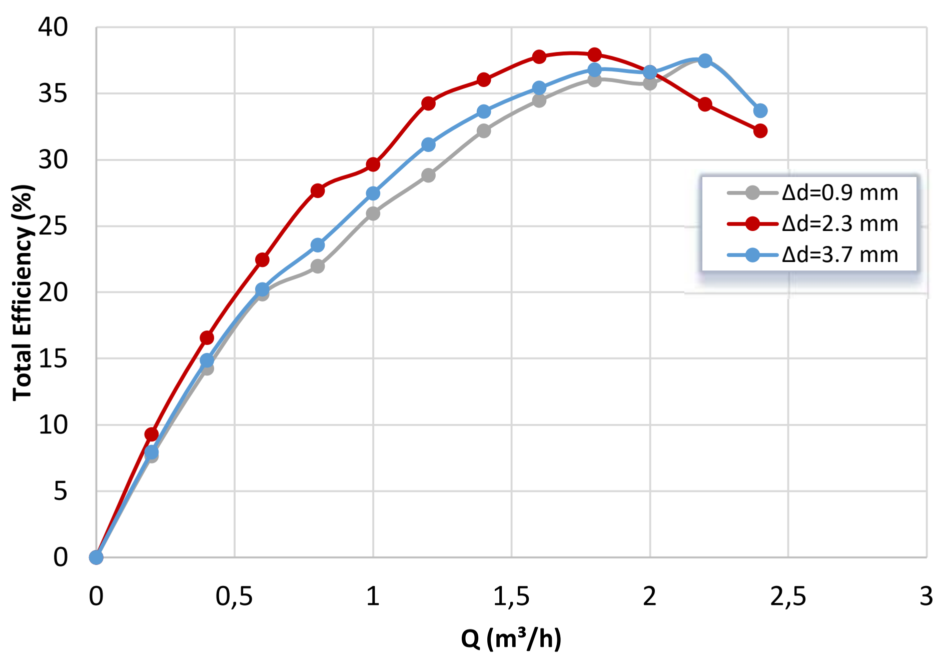

Figure 16: Variation of total pump efficiency with flow rate at different gap distances (Inclination angle 30°, Volute outlet size A_1= 15.5 mm)

Figure 15 shows the change in the head (H) of the pump with a fixed rotation speed of 3750 rpm with the flow rate. When the figure is examined, it is seen that the pump has a fixed head of 7.4 m in the flow rate range of 0 and 0.75 m³/h. In addition, it is seen that the head decreases to 3.5 m as the flow rate value increases to 2.4 m³/h. Figure 14 shows the change in the power ($P_{network}$) drawn by the pump from the network with the flow rate. Here, it is seen that the $P_{network}$ value, which is 42 Watts at the flow rate value of 0 m³/h, shows an approximately linear increase, and reaches to 65 Watts at the flow rate value of 2.4 m³/h.

3.4.2 Effects of the Volute Outlet Size on Pump Performance

The results of both cross-section A_1 and A_2 are shown in Figure 17, Figure 18 and Figure 19. Unexpectedly, the A_1 has higher head values and lower consumed power. So that efficiency is 2-3 percent better than A_2's, as shown in Figure 19. Consequently, continuing with A_1 cross-section, which has a small exit cross-sectional area, will give us a more efficient pump casing.

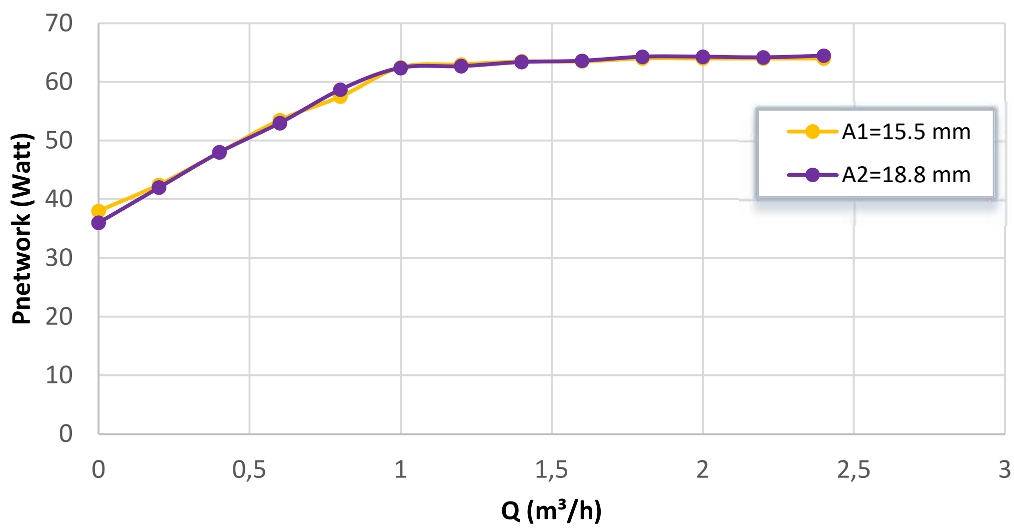

Figure 17: Variation of power consumption with flow rate at different volute outlet size. (Inclination angle α_1=30°, gap distance Δd=2.3 mm)

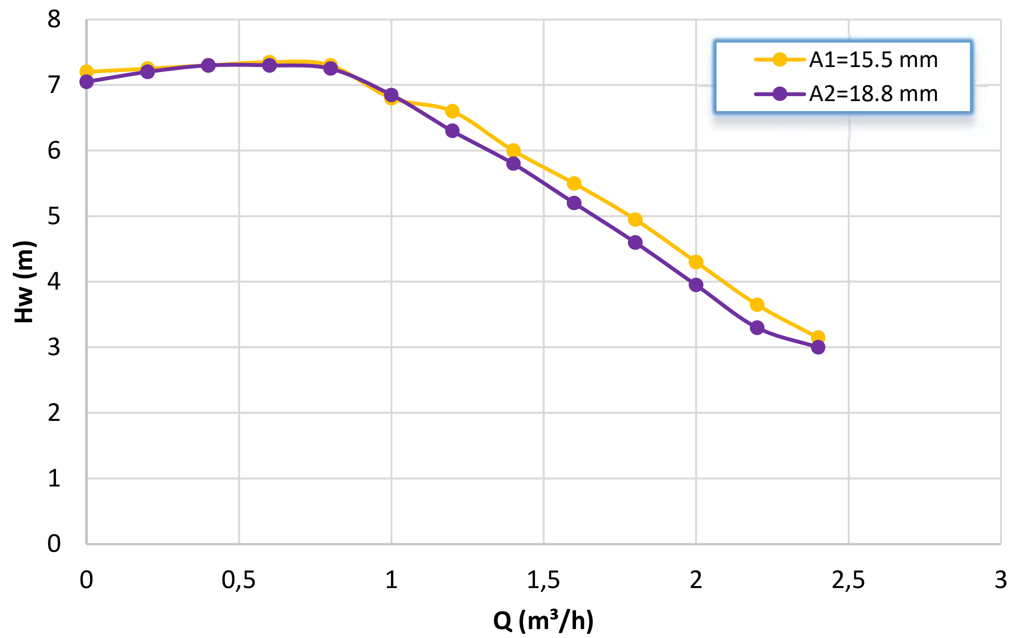

Figure 18: Variation of the pump head with flow rate at different volute outlet size. (Inclination angle α_1=30°, gap distance Δd=2.3 mm)

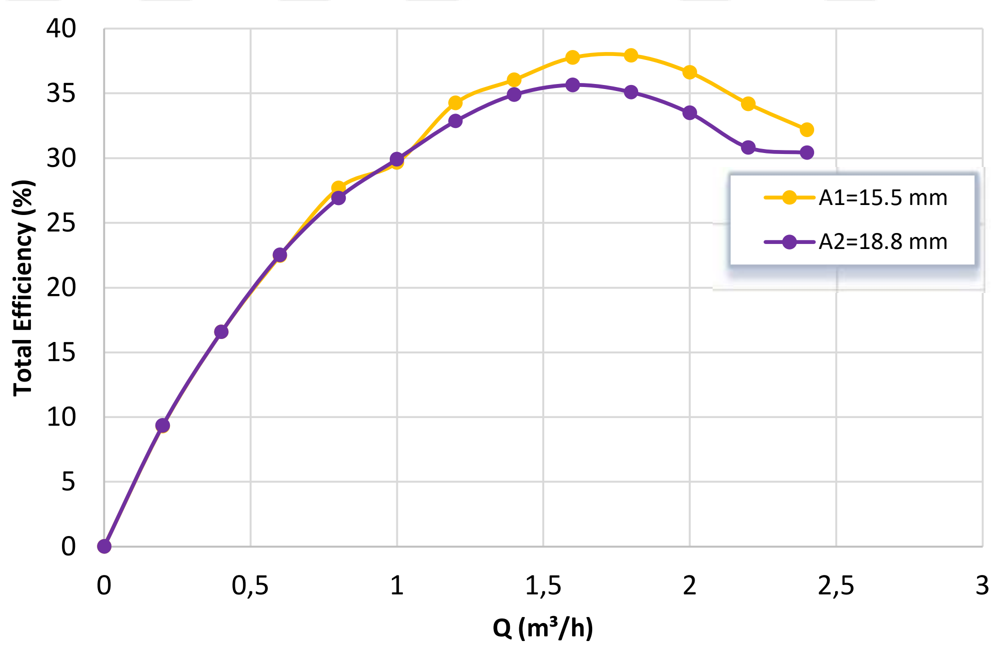

Figure 19: Variation of total pump efficiency with flow rate at different volute outlet size. (Inclination angle α_1=30°, gap distance Δd=2.3 mm)

3.4.3 Effects of the Inclination Angle of Inlet Pipe on Pump Performance

In this experiment, we look for what are the effects of the inclination angle of inlet pipe of pump casing on the performance. This experiment gives us the influence of the inlet angle on the suction. The results of the different angle (α_1 and α_2) casing are shown in the graphics below. It can be easily seen that the pump casing with α_2 has lower performance values. So, there is no reason to continue with the α_2 pump casing.

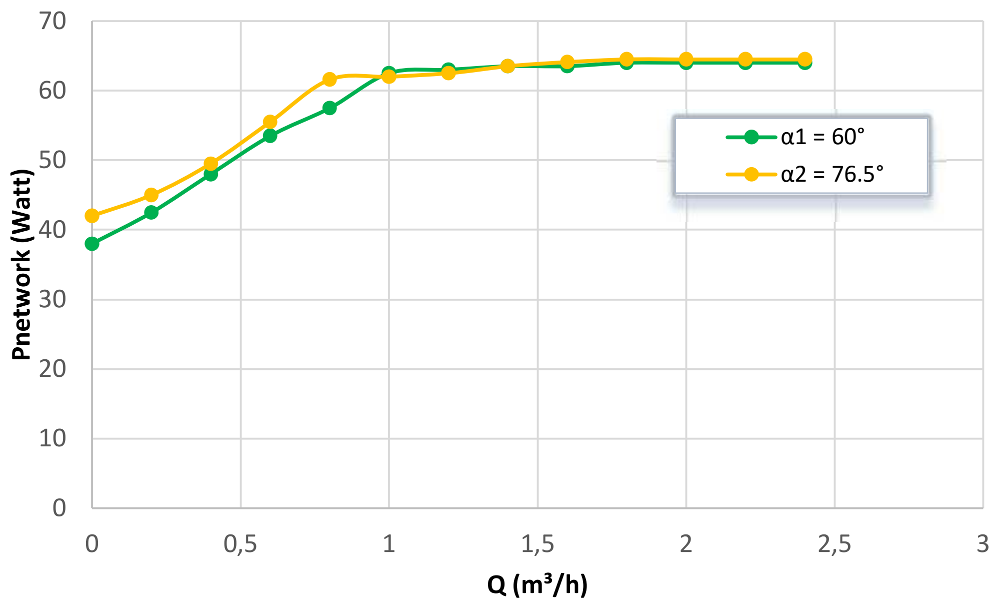

Figure 20: Variation of power consumption with flow rate at different inclination angles. (Volute outlet size A_1= 15.5 mm, gap distance Δd=2.3 mm)

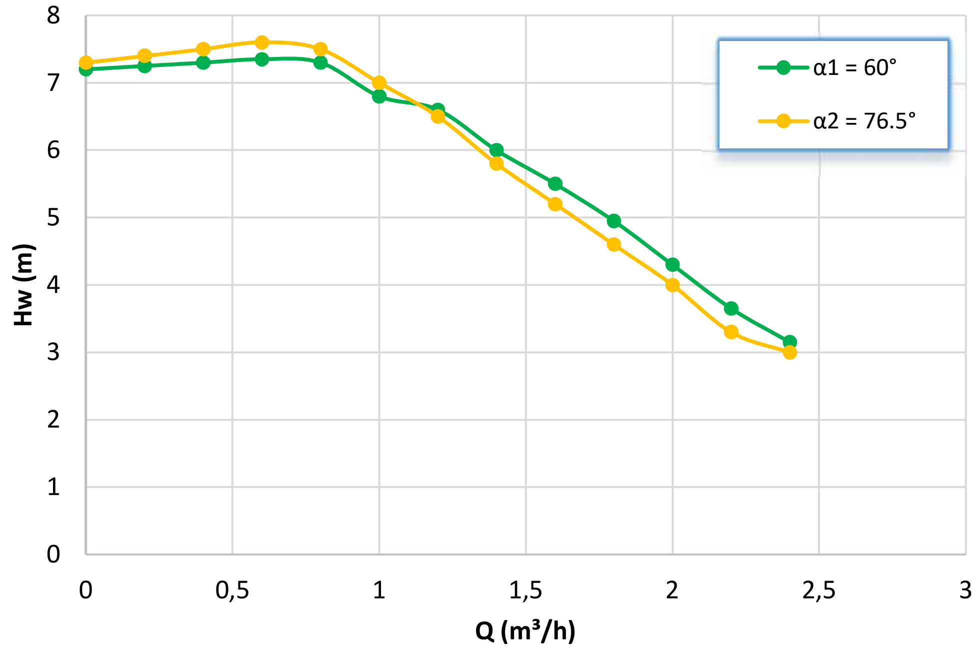

Figure 21: Variation of the pump head with flow rate at different inclination angle. (Volute outlet size A_1= 15.5 mm, gap distance Δd=2.3 mm)

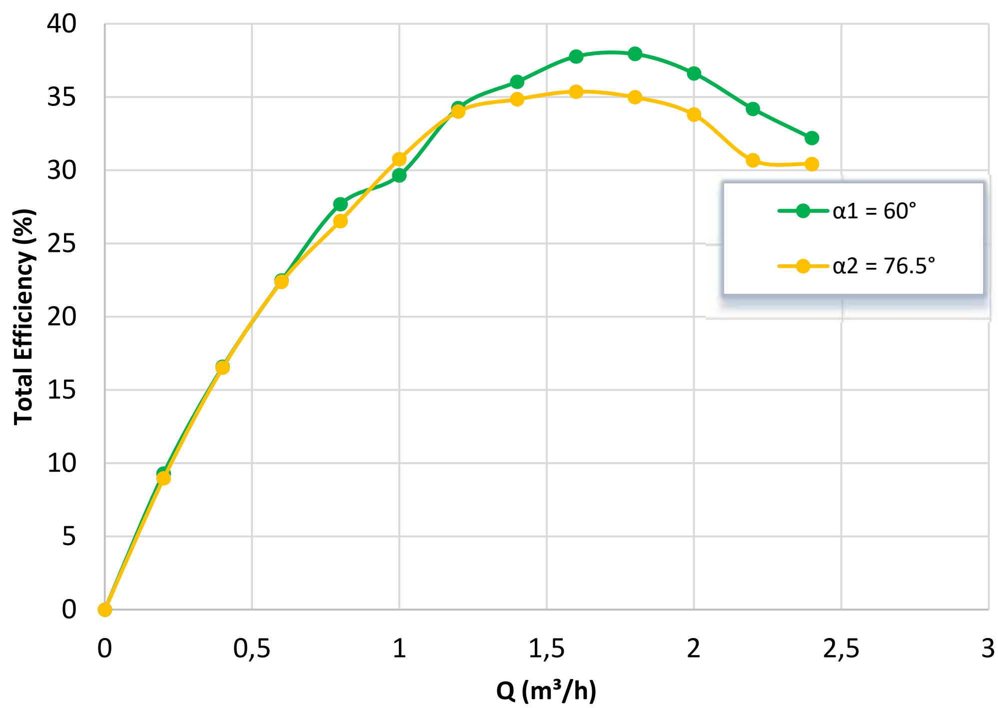

Figure 22: Variation of total pump efficiency with flow rate at different inclination angles. (Volute outlet size A_1= 15.5 mm, gap distance Δd=2.3 mm)

3.4.4 Comparison of the optimized plastic casing with the casting casing

Figure 23 shows the variation of total pump efficiency with flow rate for optimized plastic casing and casting casing. It is seen that casting the pump casing has 2 percent more efficiency. Because it has no design restriction for the production method. But plastic casing still has a big economic advantage. The production cost of plastic casing is 4£ less than casting casing. The standard lifetime of circulation pumps is five years. The cost of energy consumed during the five years cannot reach this cost difference.

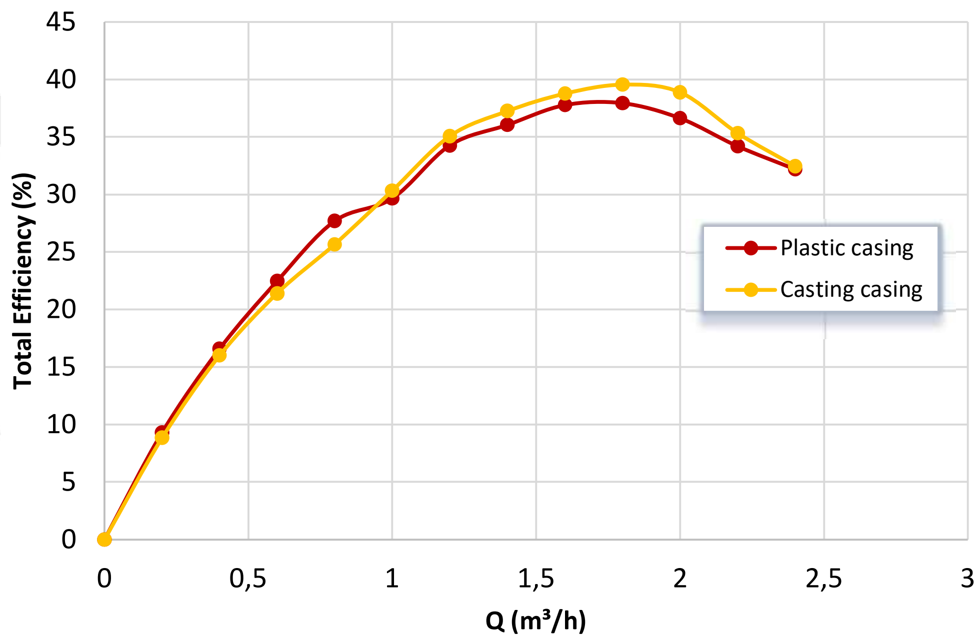

Figure 23: Efficiency results of the plastic pump casing and the casting pump casing

CHAPTER IV
NUMERICAL STUDY

The numerical simulations were carried out using a commercial computational fluid dynamics (CFD) code to solve the three-dimensional steady Navier-Stokes equations and predict the performance of the pump. With these simulations, the effects of different geometries such as suction curve geometry, the geometry at the impeller-intake interface, and volute tongue geometry on pump performance were analyzed for the optimization of the pump design.

4.1 CREATİNG PUMP FLOW GEOMETRY

The structural component of the pump includes pump volute casing, impeller, and impeller shaft. The fluid part is called the hydraulic model of centrifugal pump. The flow geometry consists of three flow domains: rotating unit, volute casing unit, and intake unit. The flow geometry is illustrated in Figure 24.

For this purpose, first, a spiral helix-volute (casing) flow geometry is designed that would direct water from the impeller outlet to the connection pipe on the discharge side of the pump. Then, the impeller region flow geometry that supports the impeller and a suction elbow flow geometry that completes this geometry, which would direct water from the connection pipe on the suction of the pump to the impeller inlet, were created. Finally, the impeller geometry is extracted from the designed flow geometries, and a three-dimensional pump flow volume solid model was created. In the design, the impeller rotation axis was positioned exactly in the middle of the body inlet and outlet axis opening given as 130 mm in Table 1.

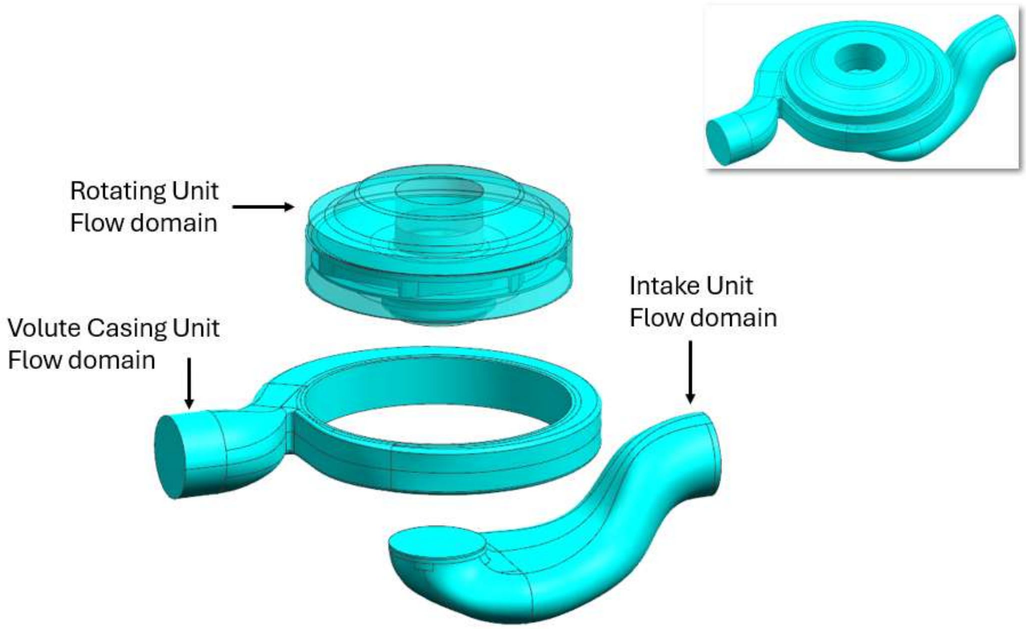

Figure 24: Flow volumes of the parts of the existing pump considered for the study.

4.2 BASIC EQUATIONS

The following assumptions were made in the solution of the equations.

- 3D flow,
- Steady flow ($\partial/\partial t=0$),
- Incompressible flow (ρ=constant),
- Gravity effect can be neglected ($g_{x,y,z}=0$),
- Turbulent flow,
- Fluid physical properties are constant (ρ=constant, μ=constant)

4.2.1 Reynolds Averaged Navier-Stokes (RANS) Equations

A numerical solution to any problem starts with the mathematical formulation of the problem. Mathematical equations of flows are obtained by applying basic laws (conservation of mass, Navier-Stokes (RANS) Equations) to a control or a system volume. To complete the mathematical formulations, boundary and initial conditions should also be expressed in terms of mathematical terms. To establish the Reynolds-averaged Navier-Stokes equations, the Reynolds decomposition is first examined. In this decomposition, the sum of the hydrodynamic quantity changes with position is equal to the sum of the pressure change, viscous forces, and body forces. This mathematical expression is given in Eq. 4.1.

Under the conditions of incompressible flow with constant dynamic viscosity (ρ=constant, μ=constant) the Navier Stoke equations can be reduced to below equations.

$$\mathrm{x}-\mathrm{d}irection: \quad \rho\left(\overline{\mathrm{w_x}}\frac{\partial\overline{\mathrm{w_x}}}{\partial \mathrm{x}}+\overline{\mathrm{w_y}}\frac{\partial\overline{\mathrm{w_x}}}{\partial \mathrm{y}}+\overline{\mathrm{w_z}}\frac{\partial\overline{\mathrm{w_x}}}{\partial \mathrm{z}}\right) = -\frac{\partial\overline{\mathrm{P}}}{\partial \mathrm{x}}+\mu\mathrm{t}\left(\frac{\partial^2\overline{\mathrm{w_x}}}{\partial \mathrm{x}^2}+\frac{\partial^2\overline{\mathrm{w_x}}}{\partial \mathrm{y}^2}+\frac{\partial^2\overline{\mathrm{w_x}}}{\partial \mathrm{z}^2}\right)+\rho\mathrm{g_x} \tag{4.1}$$

$$\mathrm{y}-\mathrm{d}irection: \quad \rho\left(\overline{\mathrm{w_x}}\frac{\partial\overline{\mathrm{w_y}}}{\partial \mathrm{x}}+\overline{\mathrm{w_y}}\frac{\partial\overline{\mathrm{w_y}}}{\partial \mathrm{y}}+\overline{\mathrm{w_z}}\frac{\partial\overline{\mathrm{w_y}}}{\partial \mathrm{z}}\right) = -\frac{\partial\overline{\mathrm{P}}}{\partial \mathrm{y}}+\mu\mathrm{t}\left(\frac{\partial^2\overline{\mathrm{w_y}}}{\partial \mathrm{x}^2}+\frac{\partial^2\overline{\mathrm{w_y}}}{\partial \mathrm{y}^2}+\frac{\partial^2\overline{\mathrm{w_y}}}{\partial \mathrm{z}^2}\right)+\rho\mathrm{g_y} \tag{4.2}$$

$$\mathrm{z}-\mathrm{d}irection: \quad \rho\left(\overline{\mathrm{w_x}}\frac{\partial\overline{\mathrm{w_z}}}{\partial \mathrm{x}}+\overline{\mathrm{w_y}}\frac{\partial\overline{\mathrm{w_z}}}{\partial \mathrm{y}}+\overline{\mathrm{w_z}}\frac{\partial\overline{\mathrm{w_z}}}{\partial \mathrm{z}}\right) = -\frac{\partial\overline{\mathrm{P}}}{\partial \mathrm{z}}+\mu\mathrm{t}\left(\frac{\partial^2\overline{\mathrm{w_z}}}{\partial \mathrm{x}^2}+\frac{\partial^2\overline{\mathrm{w_z}}}{\partial \mathrm{y}^2}+\frac{\partial^2\overline{\mathrm{w_z}}}{\partial \mathrm{z}^2}\right)+\rho\mathrm{g_z} \tag{4.3}$$

4.2.2 k-omega SST Turbulence Model

In this turbulence method, ω is an inverse time scale and is connected with turbulence.

It resolves two additional equations:

– A recast form of the k equation used in the k-ε model.

– A transport equation for ω.

The turbulent viscosity is defined as:

Its numerical performance is comparable with that of k-ε models. It shares some of the same shortcomings, e.g., isotropic μ_t assumption.

$$\mu_t = \rho\frac{k}{\omega} \tag{4.4}$$

μ_t = turbulent viscosity (Pa.s)

k = turbulent kinetic energy (J/kg)

4.3 BOUNDARY CONDITIONS

In a steady state, the simulation is set up using the multireference frame method, where the impeller is set in the rotating reference frame and the volute in the fixed reference frame, and correlated with one another by the "frozen rotor." The meshes of different domains are connected using interfaces. At these interfaces, the flow fluxes are calculated from linear interpolation across the two sides, fully implicit and fully conservative in flow fluxes. Boundary conditions are considered together with real operating conditions, as specified in Table 4. Mass flow rate outlet at the pump outlet and pressure inlet boundary at the pump inlet. Smooth nonslip walls conditions have been imposed upon all the physical surfaces, with the exception of the interfaces between various components. Boundary conditions are shown in Fig. 25.

The fluid is water, with a temperature of 20°C, density of 998.2 kg/m^3, and viscosity of 1.003x10^{-3} Pa.s.

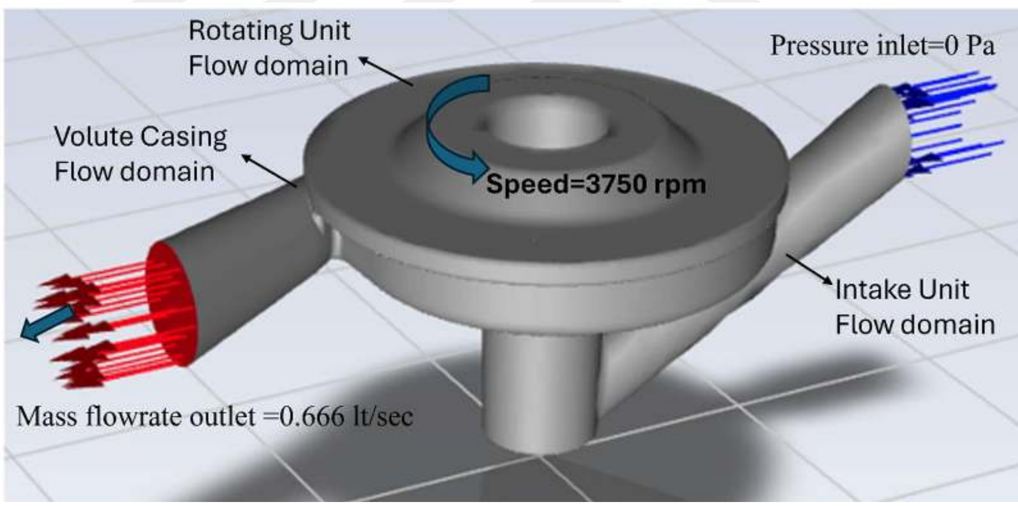

Figure 25: Boundary conditions of injection molded pump casing pump model

4.4 NUMERICAL SOLUTION

The full 3D incompressible Navier-Stokes equations are solved in ANSYS-CFX code. The governing equations have been discretized employing the finite volume method, and high-resolution algorithm has been employed to solve the equations. Turbulence has been modeled employing k-omega SST (shear stress transport) turbulence model. Scheme for space and pressure is second order accuracy. Pressure-velocity coupling has been solved employing the SIMPLEC algorithm.

4.4.1 Meshing and Preparing Model

For numerical modeling, unstructured tetrahedral and polyhedral meshing for all computational domains is utilized. This is due to the fact that unstructured mesh is utilized in the current analysis due to complexity and irregular shape of the intake section, impeller and volute geometry. Polyhedral mesh is generated in the Ansys Fluent meshing program to increase the mesh quality. The number of mesh cells is significantly reduced with polyhedral mesh. As a result, the solving time is dramatically decreased.

The meshes of three calculation domains, the intake section, impeller and volute casing, are solved separately. The calculation domains at the inlet of the intake section and outlet of the volute section are extended to accommodate recirculation space. The reverse flows are, therefore, not created at the inlet and the outlet. The extension is equal to two times the inlet and volute outlet diameter and is equivalent to the actual location of pressure measurement in the test rig.

The inflation layers are produced on the walls with 10 layers and 1.2 growth ratio. These layers allow us to calculate the boundary flows. The curvatures are captured by activating the curvature property. So, the real pump geometry surfaces are achieved with good accuracy. The proximity property is also applied to small gaps to produce a minimum of 3 cells for the thinnest regions. So, all details are captured in the simulation analysis.

A local mesh refinement is employed at regions around volute tongue area, leading and trailing edge of impeller blade with the aim of precisely capturing the structure of the flow field. This is because variation of flow field properties such as pressure and velocity at these regions is expected to be high.

Figure 26 and Figure 27 show the mesh assembly of the intake, impeller, and volute sections. The mesh quality is shown in Figure 28. The orthogonal quality must be above at least 0.1 for precise simulation. In our mesh model, the orthogonal quality is 0.12 for the impeller that has the most complex surfaces. The skewness quality must be below at least 0.9 for an accurate result. In our case, the skewness quality of the surface is below 0.7.

The number of elements used in the numerical simulation is fixed once the mesh independence study has been done. The subsequent sections will contain results of the mesh independence study.

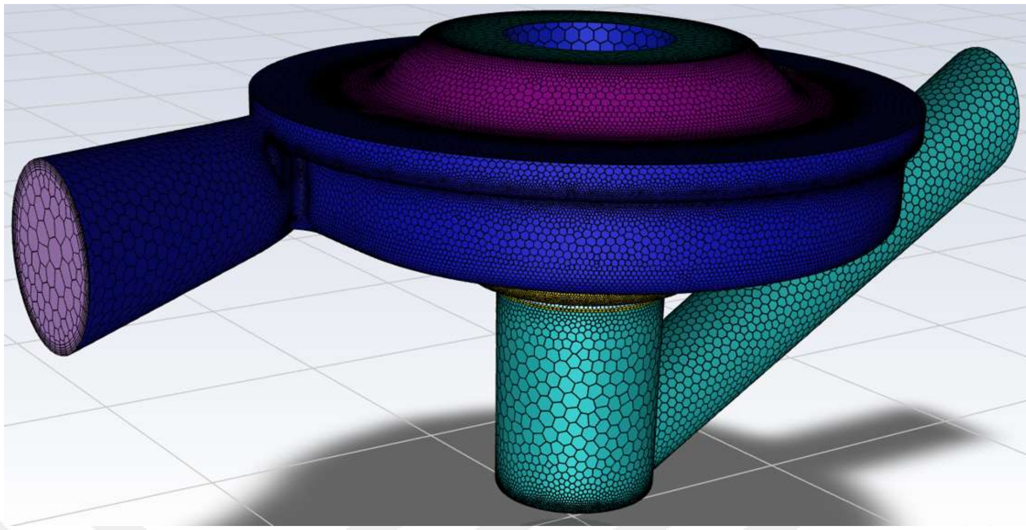

Figure 26: Polyhedral mesh

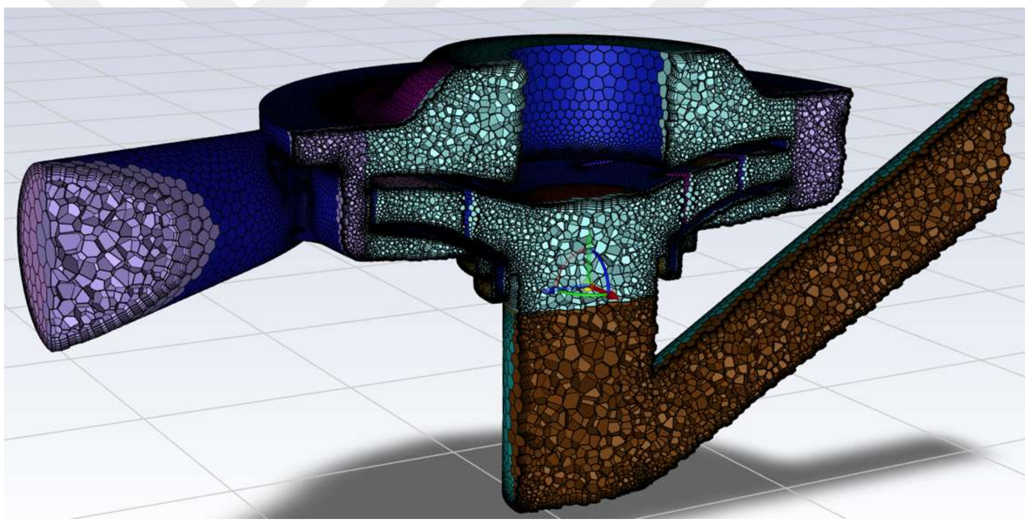

Figure 27: Polyhedral mesh section view with the inflation layers

name	id	cells (quality < 0.10)	minimum quality	cell count
part-3:82887	82887	0	0.20314155	74544
part-1:82884	82884	0	0.22293494	484423
part-2:82881	82881	0	0.11872116	1346475

name	id	cells (quality < 0.10)	minimum quality	cell count
Overall Summary	none	0	0.11872116	1905442

[Quality Measure : Orthogonal Quality]

Figure 28: Orthogonal quality values and number of cells of polyhedral mesh

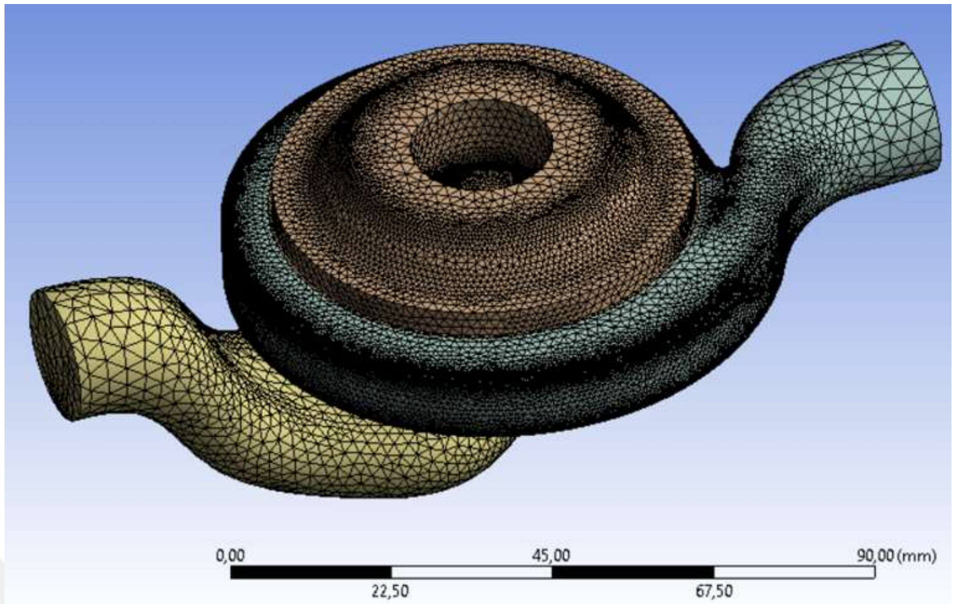

Figure 29: Hexagonal mesh

4.5 NUMERICAL CALCULATION AND VALIDATION

As a result of solving the basic equations given in Section 4.4 with appropriate boundary conditions, the velocity and pressure distribution of the flow are obtained. Using the velocity and pressure distribution obtained, the torque applied by the impeller to the fluid is calculated. In addition, the pump head is determined by taking the difference of the total pressures at the inlet and outlet sections. After determining the flow rate, torque and head, the values of the pump performance characteristic parameters such as shaft power, hydraulic power, hydraulic efficiency, etc. are calculated.

4.5.1 Convergence, Iteration Independence and Mass Conservation Control

Maximum residuals are set to 10^{-5}, and the torque value that affects the impeller surface and the head value that is calculated from the static pressure value at the pump inlet and outlet are also monitored. When the overall imbalance of all monitors is less than 0.1% or the maximum residuals are reached, the simulation was considered steady and convergent. In addition, the difference between the flow rates read at the pump inlet and outlet was checked to be very close to zero due to the conservation of mass.

Table 9: The conservation of mass control values

Pump inlet mass flowrate	Pump outlet mass flowrate	The difference between pump inlet and outlet
0,6665 kg/sec	0,6666 kg/sec	1e -04 ≅ 0

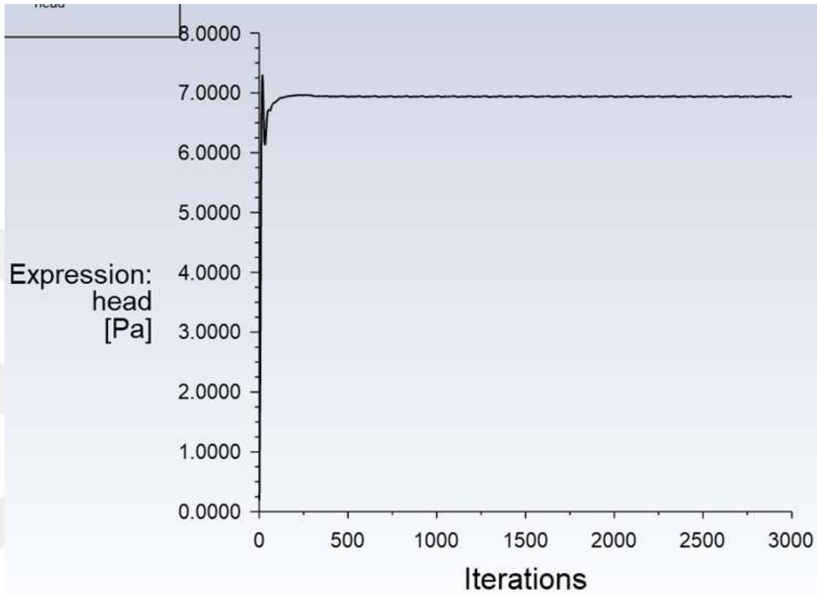

Figure 30: Head-pressure value and numbers of iteration graph

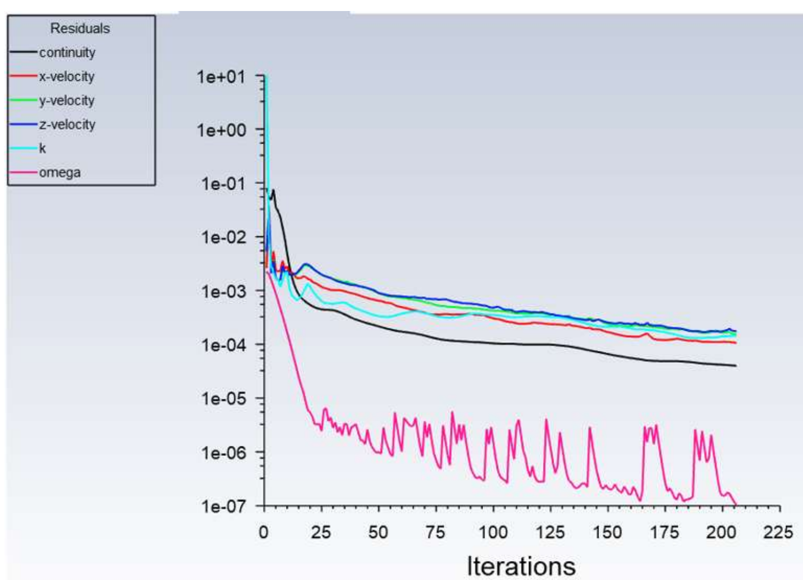

Figure 31: Residuals value and numbers of iteration graph

4.5.2 Independence of the Solution from the Number of Node

The solutions for the same pump condition were repeated with different solution node counts to determine the appropriate solution node number. The solution node number, where the solution results become independent of the solution node number, was used for all mesh structures in the numerical study. To obtain a solution independent of the solution node number, simulations were performed by taking the densities of the elements in the created solution mesh at different values without changing the hierarchy. The mesh structure that gives the most appropriate solution node number, was determined by examining the results obtained. In the examination, it was determined that the most appropriate solution, node number was around 6.0e +6.

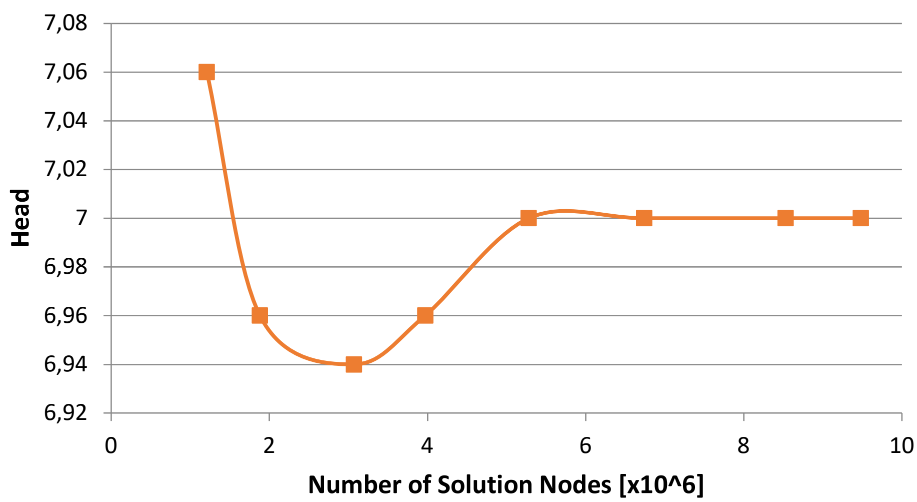

Figure 32: Independence of the solution from the number of node graph

4.6 PERFORMANCE EVALUATION AND VALIDATION OF THE RESULTS

At different flow rates, the pump's overall performance was obtained by numerical simulations and matched with experimental findings. Experimental findings compared to the numerical findings have a good correspondence, especially for the shaft power.

4.6.1 Torque and Shaft Power Calculation

The pressure force acting on the impeller surfaces creates a hydrodynamic torque on the impeller. The component of the resulting hydrodynamic torque at the impeller rotation axis is the torque applied by the impeller to the fluid. In order to calculate the torque applied by the impeller to the fluid, the values of the hydrodynamic torque at each solution point taken on the impeller surfaces were added and the component of the sum at the impeller rotation axis was taken.

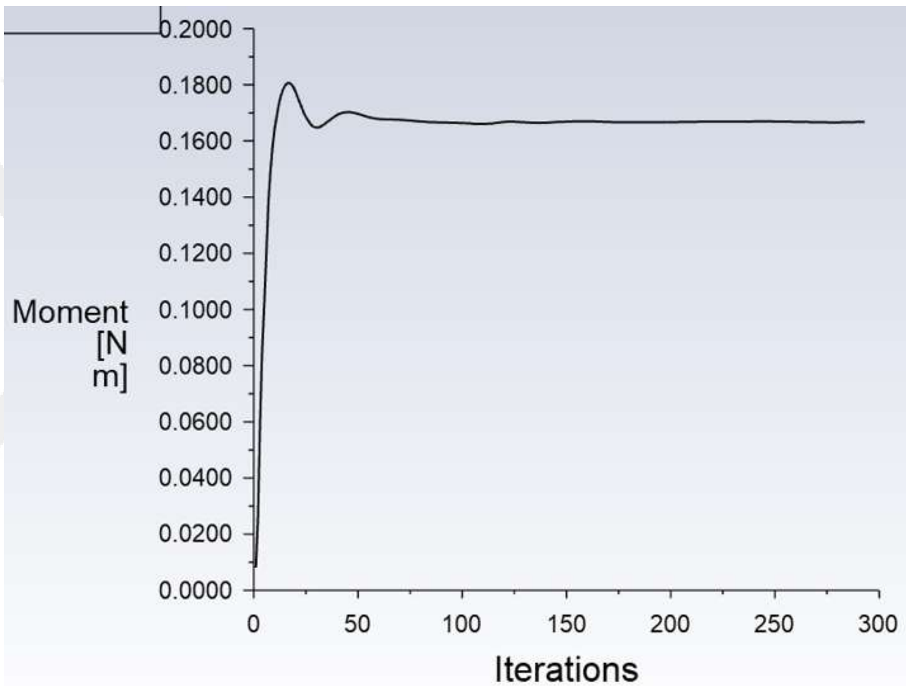

Figure 33: Moment value and numbers of iteration graph

The shaft power of the pump P_m, the torque applied to the shaft T_m and the speed N (rpm) are given in Eq.1.5. The shaft power is calculated using the torque value found in the simulation.

$$P_m = T_m\, N\, 2\pi/60 \quad \rightarrow \quad P_m = 0.167 \times 3750 \times \frac{2\pi}{60} = 65.58\ \mathrm{W} \qquad (4.5)$$

4.6.2 Hydraulic Power Calculation

Hydraulic power P_h is the power transferred to the fluid by the pump impeller, and the power has created a pressure increase (head) in the fluid. From here, P_h can be calculated from Eq. 1.4 using the values of flow rate Q, head H, gravitational acceleration g, and the density of the fluid.

$$P_h = \rho\, g\, H\, Q \;\rightarrow\; P_h = 998 \times 9.81 \times 7 \times 2.4/3600 = 45.7 \text{ W} \tag{4.6}$$

4.6.3 Pump Efficiency Calculation

The pump hydraulic efficiency from the simulation results can be found using Eq. 1.7 as below:

$$\left.\eta_h\right)_{simulation} = P_h/P_m \;\rightarrow\; \eta_p = 45.7 / 65.58 = 0.69 \tag{4.7}$$

At design flow point, the simulation head is 7 m and pump hydraulic efficiency is 69%. The total efficiency obtained from the experimental results, the hydraulic efficiency can be obtained using the assumed values of leakage, mechanic, electric motor and driver efficiencies as follows:

$$\eta_T = \eta_{em}\, \eta_{drv}\, \eta_m \eta_l \eta_h \;\rightarrow \left.\eta_h\right)_{Exp} = \eta_T / (\eta_{em}\, \eta_{drv}\, \eta_m \eta_l) \tag{4.8}$$

From the experimental results total efficiency was obtained as 37%. The electrical motor efficiency was assumed as 0.83 for a permanent magnet electronic motor. The electronic board efficiency of the driver was assumed 0.95 because of electrical component heat losses on the board. The mechanical efficiency of the pump was taken as 0.72 because of the bearing and sealing losses. Using these experimental values, hydraulic efficiency is obtained as below:

$$\left.\eta_h\right)_{Exp} = 0.37 / (0.83 \times\ 0.95 \times\ 0.72 \times 1) = 0.65 \tag{4.9}$$

For the flow rate 0f 2.4 m^3/sec considered, hydraulic efficiency obtained from experimental study (0.65) and numerical simulation (0.69) are consistent with each other. It is clearly proven that the numerical methods used in this study could simulate the pump performance with %4 error.

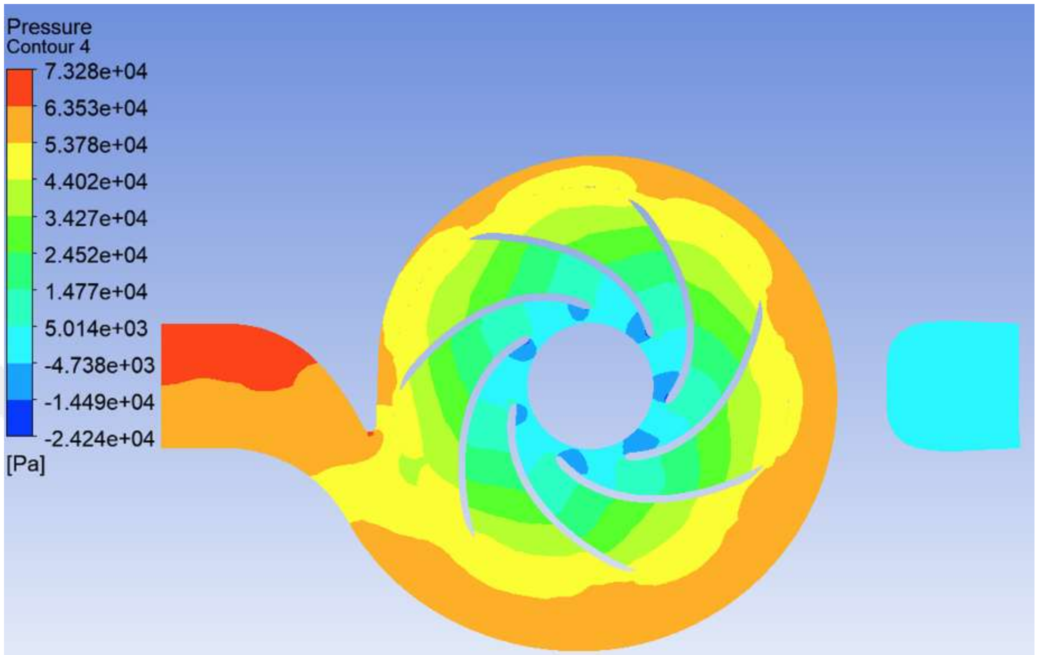

Figure 34: Pressure contours around the impeller for casting pump casing

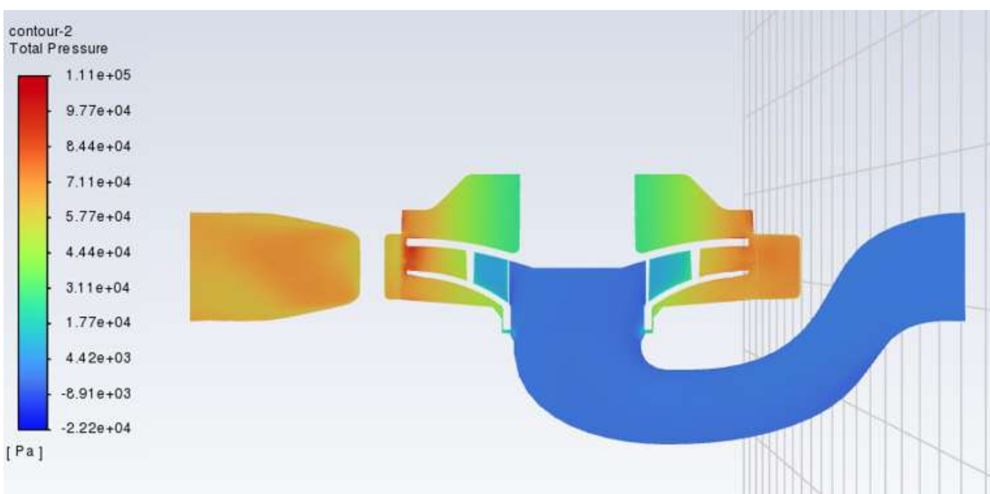

Figure 35: Pressure contours around the pump for casting pump casing

4.7 MECHANICAL ANALYSIS

The pump structural calculation is carried out by static structural analysis, which is performed by Ansys mechanical software. The pump volute casing is made of glass fiber reinforced polyamide material. Its elastic modulus is 10000 MPa, and density is 1360 kg/m3. This material is used for glass fiber reinforced injection molding grade for machinery components and housings of high stiffness and dimensional stability.

Figure 37 shows the mechanical behaviors of the composite casing under 25 bar pressure. It is clearly stated that the casing has enough stiffness under this pressure load.

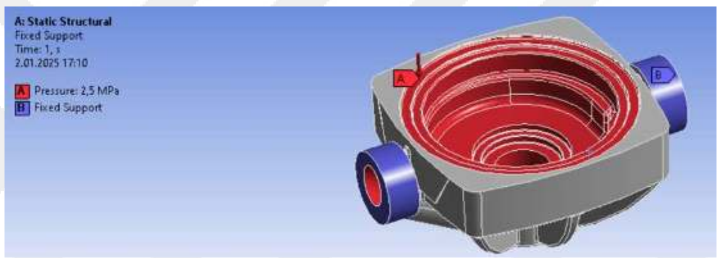

Figure 36: The surfaces that applied pressure of 25 bar

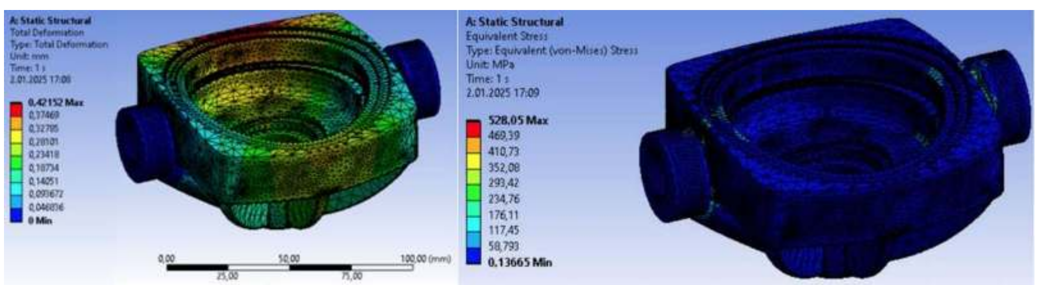

Figure 37: Deformation and equivalent stress distribution on casing

CHAPTER V
CONCLUSIONS

In the present study, optimization of the centrifugal pump casing was carried out by experimental and numerical analysis. Redesigning of the pump casing was done according to the molding principle of the plastic injection manufacturing process. Numerical methods for prediction of the pump performance were introduced, such as meshes, boundary conditions, and turbulence models. The original pump was experimentally tested in a centrifugal pump test rig. After that, the numerical results of the original pump were compared with the experimental results, and the two methods' comparisons are in good agreement.

Three different gaps are analyzed during the experimental tests. The experimental studies show that the impeller-tongue gab (Δd) has a significantly important role in efficiency. The optimum gap is achieved with the gap value 2.3 mm. This result validates the literature work on cut water diameter calculations mentioned in this study.

The inclination angle of inlet pipe and volute outlet size are investigated. It was seen during the test that the inclination angle has no important effect on the performance of the pump. The big volute outlet size also has a negative effect on pump performance.

An optimally efficient centrifugal pump casing that can be produced by the injection molding technique is obtained after all investigations and various design iterations (the three different impeller-tongue gaps (Δd), the two different inclination angle of inlet pipe and the two different volute outlet sizes).

As future work, designing smaller plastic pump casings that work at higher speeds to obtain the same head could be one topic. Another topic could be that the number of parameters can be increased to determine the optimum and precise parameter by numerical methods.

REFERENCES

AYAD A. Farid, ABDALLA H. M. and EL-AZM A. Abou (2015), "Study of the Effect of Impeller Side Clearance on the Centrifugal Pump Performance Using CFD", *Proceedings of the ASME 2015 International Mechanical Engineering Congress and Exposition IMECE2015*, Texas.

GULICH Johann Friedrich (2010), *Centrifugal Pumps*, Second Edition, Springer, USA.

KARAKAYA Uğur Can (2022), *Development of centrifugal pump for electric vehicle battery thermal management system* (Master Thesis), Istanbul Technical University Graduate School of Engineering and Science, İstanbul.

KSB COMPANY (2025), *KSB Centrifugal Pump Lexicon*, https://www.ksb.com/en-global/centrifugal-pump-lexicon/article/head-1115612, DoA. 07.09.2025.

MAHDI M., RASEKH R. and SAJADI V. (2022), "Unsteady Fluid Flow Analysis of Tongue Geometry in a Centrifugal Pump at Design and Off-design Conditions", *Journal of Applied Fluid Mechanics,* Vol. 15, No. 6, pp. 1851-1867.

MENTZOS Michalis Dimitrios, FILIOS Andronicos E., MARGARIS Dionisios P. and PAPANIKAS Dimitrios G. (2004), ''A Numerical Simulation of the Impeller-Volute Interaction in a Centrifugal Pump'', *1st International Conference "From Scientific Computing to Computational Engineering",* Athens, Greece.

NANDAN Ruchir, PASHA S. M., ASHISH D. and NOOKARAJU B. Ch. (2023), ''Computational Fluid Dynamics (CFD) Analysis of Centrifugal Pumps'', *E3S Web of Conferences,* Vol. 391, DOI: 10.1051/e3sconf/202339101088.

ORO J.M. Fernandez, PEROTTI R. Barrio, VEGA M. Galdo and GONZALEZ J. (2023), "Effect of the radial gap size on the deterministic flow in a centrifugal pump due to impeller-tongue interactions", Vol. 278, Part A, DOI: 10.1016/j.energy.2023.127820.

ÖZTÜRK Adnan, AYDIN Kadir, SAHİN Besir and PINARBASI Ali (2009), "Effect of impeller-diffuser radial gap ratio in a centrifugal pump", *Journal of Scientific & Industrial Research*, Vol. 68, pp.203-213.

ÖZBILGIN Onur (2017), *Circulation Pump Design and Performance Analysis Using CFD Technique* (Master Thesis), Gazi University Graduate School of Engineering and Science, Ankara.

SRINIVASAN K. M. (2008), *Rotodynamic Pumps (Centrifugal and Axial)*, First Edition, New Age International, India.

TURKISH STANDARD INSTITUTE (2012), *Rotodynamic pumps - Hydraulic performance acceptance tests - Grades 1, 2 and 3,* TS EN ISO 9906:2012-07.